Tgfbr1 regulates lateral plate mesoderm and endoderm reorganization during the trunk to tail transition

Anastasiia Lozovska[1], Ana Nóvoa1, Ying-Yi Kuo[2], Arnon D. Jurberg[1#], Gabriel G. Martins[1], Anna-Katerina Hadjantonakis[2] & Moises Mallo[1*]

1 Instituto Gulbenkian de Ciência, Rua da Quinta Grande 6, 2780-156 Oeiras, Portugal

2 Developmental Biology Program, Sloan Kettering Institute, Memorial Sloan Kettering Cancer Center, New York, NY, USA

Current address: Universidade Estácio de Sá (UNESA)/Instituto de Educação Médica (IDOMED) - Campus Vista Carioca, 20071-004 Rio de Janeiro/RJ, Brazil, and Laboratório de Animais Transgênicos, Universidade Federal do Rio de Janeiro (UFRJ), 21941-599 Rio de Janeiro/RJ, Brazil.

* lead contact: mallo @igc.gulbenkian.pt

Key words: trunk to tail transition; Tgfbr1 signaling; Isl1; lateral plate mesoderm; endoderm

ABSTRACT

During the trunk to tail transition the mammalian embryo builds the outlets for the intestinal and urogenital tracts, lays down the primordia for the hindlimb and external genitalia, and switches from the epiblast/primitive streak to the tailbud as the driver of axial extension. Genetic and molecular data indicate that *Tgfbr1* is a key regulator of the trunk to tail transition. *Tgfbr1* has been shown to control the switch of the neuro mesodermal-competent cells from the epiblast to the chordo-neural hinge to generate the tail bud. We now show that Tgfbr1 signaling also controls the remodeling of the lateral plate mesoderm (LPM) and of the embryonic endoderm associated with the trunk to tail transition. In the absence of *Tgfbr1* the two LPM layers do not converge at the end of the trunk, extending instead as separate layers enclosing the celomic cavity until the caudal embryonic extremity, and failing to activate markers of primordia for the hindlimb and external genitalia. However, this extended LPM, does not exhibit the molecular signatures characteristic of this tissue in the trunk. The vascular remodeling involving the dorsal aorta and the umbilical artery leading to the connection between embryonic and extraembryonic circulation was also affected in the *Tgfbr1* mutant embryos. Similar alterations in the LPM and vascular system were also observed in *Isl1* null mutants, indicating that this factor acts in the regulatory cascade downstream of *Tgfbr1* in LPM-derived tissues. In addition, in the absence of *Tgfbr1* the embryonic endoderm fails to expand to form the endodermal cloaca and to extend posteriorly to generate the tail gut. We present evidence suggesting that the remodeling activity of *Tgfbr1* in the LPM and endoderm results from the control of the posterior primitive streak fate after its regression during the trunk to tail transition. Our data, together with previously reported observations, place *Tgfbr1* at the top of the regulatory processes controlling the trunk to tail transition.

INTRODUCTION

The transition from trunk to tail development is a complex process resulting in major changes in the general structure of the embryo, also involving a switch in the mechanisms regulating axial extension. Extension through the trunk is driven by axial progenitors located within the epiblast, that generate the spinal cord, the embryonic gut, and the different mesodermal compartments (Binagui-Casas et al., 2021; Cambray and Wilson, 2007; Henrique et al., 2015; Steventon and Martinez Arias, 2017; Tsakiridis and Wilson, 2015; Wilson et al., 2009a; Wymeersch et al., 2021). At

this stage, the caudal end of the mouse embryo is occupied by the allantois that will play an essential role in the connection between embryonic and extraembryonic structures (Arora and Papaioannou, 2012; Rodriguez and Downs, 2017). The transition to tail development is associated with changes in the global anatomy of the caudal end of the embryo, involving the progressive anterior relocation of the allantois along the ventral side of the embryo. During this process, the tail bud forms at the dorsal and posterior end of the embryo, and replaces the epiblast/primitive streak (PS) as the main driver of axial extension (Henrique et al., 2015; Wilson et al., 2009a). Formation of the tail bud results from changes in the progenitors generating the neural and paraxial mesodermal structures, the so-called neuro-mesodermal competent (NMC) population, which relocates from the epiblast to the chordo-neural hinge (CNH) (Binagui-Casas et al., 2021; Cambray and Wilson, 2007; Wymeersch et al., 2021).

At this stage, the lateral plate mesoderm (LPM) also undergoes a major reorganization. This mesodermal compartment, generated by progenitors situated at the caudal region of the epiblast and PS (Wymeersch et al., 2021, 2019, 2016) is composed of two layers: a ventral splanchnopleure, which contributes to the formation of the various body organs, as well as their vascularization, and a lateral somatopleure involved in the formation of the body wall (Prummel et al., 2020). These two layers delimit the celomic cavity, which will hold the animal's internal organs. During allantois relocation, the two LPM layers converge towards the midline, ending the celomic cavity and marking the posterior border of the trunk. This remodeling of the caudal part of the embryo is associated with the induction of the hindlimbs from the somatopleure (Tickle, 2015), and the generation of the pericloacal mesenchyme, the primordium of the genital tuberculum (GT) (Cohn, 2011; Yamada et al., 2006), from the ventral lateral mesoderm (VLM) posterior to the allantois (Tschopp et al., 2014).

Concomitant with the reorganization of the embryonic mesoderm, the transition from trunk to tail development also involves major changes in the embryonic endoderm and in the vascularization that will connect embryonic and extraembryonic structures. When the allantois relocates, the embryonic endoderm, whose posterior end reaches the base of the allantois, invaginates forming a cavity that will originate the cloaca, an endodermal expansion that becomes the common end of the excretory, intestinal, and genital tracts (Huang et al., 2016; Matsumaru et al., 2015). In the mouse embryo, the embryonic endoderm then expands further caudally to generate the tail gut, a transient structure with unknown function. The region of the posterior visceral (extra-embryonic)

endoderm abutting the allantois is thought to facilitate the invagination and growth of the embryonic endoderm (Rodriguez and Downs, 2017) and contribute to the hindgut epithelium (Kwon et al., 2008; Nowotschin et al., 2019).

The major blood vessels also become reorganized with the relocation of the allantois. The caudal end of the paired dorsal aortae (DA) merge and connect with the umbilical artery generated within the allantois (Arora and Papaioannou, 2012; Downs and Rodriguez, 2020). As the allantois move forward, the caudal end of the DA bends to form the recurved dorsal aorta (rDA). It is thought that this process requires the generation of a vessel of confluence from the caudal end of the PS abutting the allantois, which will constitute a major part of the rDA (Downs and Rodriguez, 2020; Rodriguez and Downs, 2017). Reorganization of the DA/umbilical artery connection will generate the blood vessels linking the embryo with the placenta and will also generate the arteries that will provide irrigation to the hindlimbs.

Molecular and genetic data indicate that Gdf11 signaling is an integral component of the gene regulatory network controlling the trunk to tail transition (Aires et al., 2019; Jurberg et al., 2013; Matsubara et al., 2017; McPherron et al., 2009, 1999). Gdf11 activity is predominantly mediated by transforming grow factor β receptor 1 (Tgfbr1) (also known as Alk5) (Andersson et al., 2006). Indeed, premature expression of a constitutively active form of Tgfbr1 promotes early execution of the trunk to tail transition program (Jurberg et al., 2013). In addition, *Tgfbr1* is required to trigger formation of the tail bud by promoting, together with *Snai1*, an incomplete epithelial to mesenchymal transformation (EMT) in the NMC population within the epiblast (Dias et al., 2020). In the present study we show that, in addition to the lack of molecular signals for the induction of the hindlimbs and the GT, the LPM of *Tgfbr1* null mutants fail to converge leading to the posterior extension of the celomic cavity. In addition, the mutants fail to generate a cloacal cavity and to extend the endodermal tube to form the tail gut. Also, the connection between the embryonic and extraembryonic vascular systems fails to undergo normal reorganization, resulting in the expansion of the paired dorsal aorta to reach the caudal end of the embryo. We also provide evidence indicating that *Isl1* is the key functional downstream target of *Tgfbr1* for the reorganization of the LPM and vascular tissues during the trunk to tail transition, acting on the posterior PS/allantois. *Isl1* controls PS fate during its regression and regulates the establishment of the embryonic-extraembryonic

connection during the ventral relocation of the allantois. Taken together, our findings indicate that *Tgfbr1* is a master regulator of the trunk to tail transition.

MATERIALS AND METHODS

Mouse lines and embryos

The *Tgfbr1*$^{+/-}$ (Dias et al., 2020), Alf-GFP (Kwon et al., 2008), ROSA26-R-gal (Soriano, 1999), ROSA26-R-EYFP (Srinivas et al., 2001) and *Isl1-cre* (Srinivas et al., 2001) used in this work have been previously described. T-str-creERT was generated by cloning the creERT cDNA, containing the SV40 polyadenylation signal obtained from the *Cdx2-creERT* construct (Jurberg et al., 2013), under the control of the PS enhancer of the Brachyury (*Tbxt*) gene (Clements et al., 1996). The construct was used to generate transgenic animals by pronuclear microinjection according to standard protocols (Hogan et al., 1994). Mutant and transgenic lines were genotyped from ear or digit biopsies incubated in 50 μL of PBND buffer (50 mM KCl, 10 mM Tris-HCl, pH 8.3, 2.5 mM $MgCl_2$, 0.1 mg/mL gelatin, 0.45% NP40, 0.45% Tween 20) supplemented with 100 μg/mL of proteinase K at 55˚C overnight. Samples were incubated at 95˚C for 15 minutes to heat-deactivate proteinase K. 1 μL of genomic DNA was used in PCR reaction with the relevant primers specified in Table 1.

Tgfbr1 null and *Isl1* null embryos were generated from intercrosses between *Tgfbr1*$^{+/-}$ and *Isl1-cre*$^{+/cre}$ mice, respectively. Embryos obtained from heterozygous crossings were genotyped from their yolk sacs. Yolk sacs were collected to 50 μL of lysis buffer (50 mM KCl, 10 mM Tris-HCl, pH8.3, 2 mM $MgCl_2$, 0.45% Tween-20, 0.45% NP40) supplemented with 100 μg/mL of proteinase K and incubated at 55˚C overnight. Samples were heat-deactivated as described above. PCR was performed using 1 μL of genomic DNA using the primers specified in Table 1.

Whole mount in situ hybridization and sectioning

Embryos were fixed in 4% paraformaldehyde in PBS (PFA) overnight, then dehydrated through a 25%, 50% and 75% series of methanol in PBT (PBS, 0,1% Tween 20), then incubated in 100% methanol. Embryos were then rehydrated through a reverse methanol/PBT series and incubated three times in PBT for at least 5 min each at room temperature. Embryos were then bleached for 1 hour in 6% hydrogen peroxide in PBT and permeabilized in 10 μg/mL of proteinase K in PBT for a time

period that depended on the embryo size. The reaction was then quenched with a 2 mg/mL solution of glycine in PBT, washed twice in PBT and postfixed in a 4% PFA and 0,2% glutaraldehyde mix for 20 minutes, followed by two washes in PBT. Hybridization was performed at 65˚C overnight in hybridization solution (50% formamide, 1.3 x SSC pH 5.5 [20 x SSC is 3M NaCl, 300 mM sodium citrate], 5 mM EDTA, 0.2 % Tween 20, 50 μg/mL yeast tRNA, 100 μg/mL heparin) containing the relevant digoxigenin-labelled antisense RNA probes. RNA probes were *in vitro* transcribed from the linearized vector for 3 hours at 37˚C with the corresponding RNA polymerase and DIG RNA Labeling Mix (Roche #11277073910). The reaction product was verified in 0,8% agarose gel and diluted in hybridization solution for further use. After hybridization, embryos were washed twice at 65˚C with hybridization solution without tRNA, heparin, and the RNA probe and then in a 1:1 mix of hybridization solution and TBST (25 mM Tris-HCl, pH 8.0, 140 mM NaCl, 2.7 mM KCl, 0.1% Tween 20) for 30 min at 65ºC. Embryos were then washed three times with TBST at room temperature, equilibrated in MABT (100 mM maleic acid, 150 mM NaCl, 0.1 % Tween-20, pH 7.5) and blocked in MABT blocking buffer [MABT containing 1% blocking reagent (Roche #11096176001)] with 10% sheep serum for 2.5 hours at room temperature. Embryos were then incubated overnight at 4ºC with a 1:2000 dilution of alkaline phosphatase-conjugated anti-digoxigenin antibody (Roche #11093274910) in MABT blocking buffer with 1% sheep serum. After extensive washes with MABT at room temperature, embryos were equilibrated in NTMT buffer (100 mM Tris HCl, pH 9.5, 50 mM $MgCl_2$, 100 mM NaCl, 0.1% Tween-20) and developed with a 1:50 dilution of NBT/BCIP solution (Roche #11681451001) in NTMT at room temperature in the dark. Stained embryos were mounted in a 0,45% gelatin, 27% bovine serum albumin (BSA), 18% sucrose mix, jellified with 1,75% glutaraldehyde and sectioned at 35 μm on a Leica Vibratome VT 1000 S.

Whole mount immunofluorescence and image processing

Embryos were fixed in 4% PFA on ice for 2 hours and then dehydrated through a 25%, 50%, 75% methanol/PBST (PBS, 0,1% Triton-X 100) series followed by 100% methanol. Embryos were then rehydrated through a reverse methanol PBST series, washed with PBST and permeabilized in 0,5% Triton-X 100 in PBS for 1 hour and incubated in 1M glycine in PBST for 30 minutes to reduce unspecific binding. After

several washes in PBST embryos were blocked in 1% BSA, 3% donkey serum in PBST at 4˚C overnight. Embryos were then incubated for 72 hours at 4˚C with the following dilutions of the primary antibodies in blocking buffer: Pecam1 1:50 (ab28364, Abcam), Keratin 8 1:100 (Troma1, developed by Dr Brulet and Dr Kemler, obtained from the NICHD Developmental Studies Hybridoma Bank maintained by the University of Iowa). Secondary antibodies were diluted 1:1000 in blocking buffer and embryos incubated for 48 hours at 4˚C. After extensive washes in PBST embryos were stained with a 1:10000 DAPI dilution in PSBT at 4˚C overnight. Embryos were then mounted on a depression slide with RapiClear 1.49 clearing reagent (SunJin lab). Embryos were imaged on a Prairie Multiphoton microscope using an Olympus 20X 1.0 NA W objective. Stacks were then digitally stitched in Fiji using the Grid/Collection stitching plugin. After removing the outliers, tissues were segmented using Amira Software.

Analysis of the contribution of the visceral endoderm to the embryonic gut

E7.5 embryos were fixed for 20 min in 4% PFA at room temperature, washed three times in PBST, and then counterstained in 5 µg/ml Hoechst and 5 U/ml phalloidin before imaging. E8.5 embryos were permeabilized in 0.5% Triton-X100 in PBS for 20 min, washed three times in PBST and incubated in blocking buffer containing 5% donkey serum (Jackson Labs) and 1% BSA in PBST for 1 h at 4 °C. Embryos were then incubated overnight at 4 °C with Epcam (cat#118202, Biolegend) (1:100) and GFP (GFP-1020, Aveslabs) (1:500) in blocking buffer. After 3 washes in PBST, embryos were incubated with secondary antibody (1:500) overnight at 4 °C, and then washed again 3 times in PBST and counterstained in 5 µg/ml Hoechst. For E9.5 and E10.5 embryos, samples were fixed for 1 h in 4% PFA at room temperature, washed three times in PBS, then dehydrated through a 25%, 50%, 75% methanol/H_2O series followed by 100% methanol. Embryos were stained with antibodies against Epcam (1:100) and GFP (1:500) using the iDISCO+ tissue clearing protocol as previously described (Renier et al., 2014), (updated at https://idisco.info/). E7.5 embryos were mounted in PBS and imaged on a Zeiss LSM880 using a Plan-Apo 20×/NA0.8 M27 objective. E8.5 embryos were mounted in FocusClear clearing reagent and imaged on a Zeiss LSM 880 using a Plan-Apo 20×/NA0.8 M27 objective. E9.5 embryos were mounted in dibenzyl ether (DBE) and imaged on a Zeiss LSM 880 using a Plan-Apo 20×/NA0.8 M27 objective and an EC Plan-NEOFLUAR 10×/NA0.3 objective. E10.5

embryos were imaged on a Luxendo MuVi SPIM light-sheet microscope using a Nikon Plan-Apo 10×/NA0.8 Glyc objective. Raw image data were processed in ZEN (Zeiss, https://www.zeiss.com/microscopy/us/products/microscope-software/zen.html), Luxendo Image Processor, or Imaris (Bitplane, http://www.bitplane.com/) software.

Ex vivo culture with DiI labelling

E9.5 embryos were dissected out in ice cold media [DMEM (Gibco®, Life Technologies)/15% FBS/11mM HEPES (Sigma)]. Stock DiI solution was prepared by dissolving aliquot of powdered CellTracker™ CM-DiI (Life technologies, C7000) in 10 μl of 96% ethanol. Working labeling solution was a 1:10 dilution of the stock solution in 0.3 M sucrose (Sigma). Embryos were injected with labeling solution in the ventral tailbud by mouth pipetting using a glass capillary and collected individually in a 24 well-plate on ice. Injected embryos were first imaged on SteREO Lumar.V12, Zeiss and then cultured for 20 h at 37˚C in a rotator bottle culture apparatus (B.T.C. Engineering, Milton, Cambridge, UK) at 37˚C, in a 65% O_2 atmosphere. Each embryo was cultured individually in a tube with 1.5 mL of DMEM/F-12, GlutaMAX™ (Gibco®, Life Technologies, 31331-028) containing 15%FBS, 11mM HEPES (Sigma) and supplemented with a penicillin/ streptomycin mixture. Cultured embryos were washed with PBS, imaged on SteREO Lumar.V12, Zeiss and fixed in 4% PFA for 1 h at room temperature. Next, embryos were permeabilized with 0,3% Tween in PBS for 1 h at room temperature. Nuclei were stained with a 1:5000 solution of DAPI in PBS for 16 h at 4˚C with rotation. Embryos were then washed in PBS, mounted on depression slides, and cleared with RapiClear 1.49 clearing reagent (SunJin lab). Imaging was done on a Prairie Multiphoton microscope using an Olympus 20X 1.0 NA W objective.

Reporter tracing with T-str-creERT transgenics.

Pregnant females from T-str-creERT and either ROSA26-R-βgal or ROSA26-R-YFP intercrosses were treated with tamoxifen (200 μl of a 1 mg/ml solution in corn oil) by oral gavage at different times from E7.5 to E8.5 and harvested at E9.5 or E10.5. When the ROSA26-R-YFP reporter was used, embryos were dissected on PBS and observed with SteREO Lumar.V12, Zeiss. When the ROSA26-R-βgal reporter was used embryos were fixed with 4% PFA at 4ºC for 30 min, then washed three times in PBS containing 0.02% Tween 20 for 10 min each at room temperature and developed

with 0.4 mg/ml X-gal in 5 mM $K_3Fe(CN)_6$, 5 mM $K_4Fe(CN)_6.3H_2O$, 2 mM $MgCl_2$, 0.02% NP40, 0.02% Tween 20, in PBS for several hours at 37ºC in the dark. The reaction was stopped with wash buffer, fixed with 4% PFA overnight and sectioned as described for the whole mount in situ-stained embryos. To test the time required to observe reporter activity upon tamoxifen treatment, pregnant females from T-str-creERT and ROSA26-R-YFP intercrosses were treated with a single tamoxifen dose and embryos recovered after 6, 8 or 10 hours after treatment and evaluated for YFP signal.

RESULTS

Tgfbr1 **is a key modulator of the caudal trunk mesoderm differentiation**

We previously showed that *Tgfbr1* null mutant embryos fail to activate markers labeling the hindlimb and GT primordia (Dias et al., 2020). We now assessed the defects of the *Tgfbr1* mutants at the axial level at which these genes become active in wild type embryos. Transverse sections through this area indicated abnormal morphology of the LPM (Fig. 1). In wild type embryos, the somatic and splanchnic LPM layers converge at the posterior region of the trunk at both sides of the developing endoderm at E9.5, ending the celomic cavity. In *Tgfbr1* mutant embryos, however, the two LPM layers, and, consequently, the coelomic cavity, continued extending from the trunk region of the embryo until its posterior end (Fig. 1 b',d'). Despite this apparent extension of the trunk LPM into the prospective hindlimb and VLM regions, molecular analyses suggested that the LPM properties in this area differed from those observed in the trunk. This was best illustrated by the expression of *Irx3* and *Foxf1*, somatic and splanchnic LPM markers, respectively (Funayama et al., 1999; Mahlapuu et al., 2001). Both markers were expressed following normal patterns in the trunk of *Tgfbr1*$^{-/-}$ embryos (Fig. 1Aa, Bb, Cc, Dd). However, in contrast to wild type controls, in *Tgfbr1* null mutant embryos these markers were not down regulated at the level of the trunk to tail transition, being *Foxf1* even clearly up regulated in this embryonic region (Fig.1B,D). In addition, their expression was no longer restricted to their respective LPM layers, and instead expanded to encompass the entire mesodermal tissue surrounding the celomic cavity. This feature was more clearly observed for *Foxf1* (Fig. Dd').

Another major mesodermal derivative affected by the absence of *Tgfbr1* was the main vascular tree, particularly the region connecting embryonic and extraembryonic

circulation. The four orifices surrounding the hindgut in E9.5 embryos observed in transverse sections, and diagnostic of the recurved dorsal aorta (rDA) (Zakin et al., 2005), were not detected in *Tgfbr1* mutants, in which only a single expanded vessel was visible on each side of the gut tube (Fig. 1Aa',Bb',Cc',Dd'). Pecam1-aided 3D reconstruction of the main blood vessels revealed that the DA of *Tgfbr1* mutant embryos was elongated posteriorly, reaching the tip of the gut tube. The posterior portion of the DA formed a vessel of enlarged diameter, as observed in the histological sections, that contrasts with the curvature characteristic of the rDA of wild type embryos (Fig. 2). The DA of the *Tgfbr1* mutants still merged with the umbilical artery, although following patterns different to those observed in control embryos. For instance, while in wild type embryos the paired rDAs remained as two independent vessels, merging just before their connection with the umbilical artery (Fig. 2b), the two paired arteries of *Tgfbr1*$^{-/-}$ embryos were fused along most of their path ventral to the endodermal tube, from the posterior embryonic tip to the umbilical artery. In addition, the allantois appeared to protrude perpendicularly to the embryo instead of following its curvature, as observed in wild type embryos (Fig. 2d).

Together, the above observations indicate that in the absence of *Tgfbr1* the mesodermal tissues derived from the lateral mesoderm fail to execute the normal differentiation routes associated with the trunk to tail transition.

Possible involvement of the posterior PS as mediator of Tgfbr1 activity

Splanchnic *Foxf1* expression depends on endodermal Shh activity (Astorga and Carlsson, 2007; Tsiairis and McMahon, 2009). The *Foxf1* expression observed in the lateral layer of the expanded LPM of *Tgfbr1* mutant embryos is separated from the endoderm by the celomic cavity, suggesting that it is likely to have a Shh-independent origin. Such *Foxf1* expression has been detected in the posterior PS/allantois of E8.5 embryos (Astorga and Carlsson, 2007; Tsiairis and McMahon, 2009), where it plays a role in vasculogenesis (Astorga and Carlsson, 2007). Reorganization of the vascular system to connect the embryonic and extraembryonic circulation occurs within the emergent VLM as the allantois becomes displaced anteriorly during the trunk to tail transition (Downs and Rodriguez, 2020; Rodriguez and Downs, 2017). From a functional perspective, *Foxf1* expression in the VLM is likely to derive from its expression domain in the posterior PS/allantois. *Foxf1* expression in the posterior PS/allantois is not affected by the absence of *Tgfbr1* (Fig. 3A,B), consistent with the

apparent dispensability of *Tgfbr1* activity in axial tissues before the transition to tail development. Given the absence of VLM in *Tgfbr1*$^{-/-}$ embryos, the *Foxf1*- positive cells in the extended LPM might represent the derivatives of posterior PS/allantois cells that failed to enter their normal fates, which instead become intermingled with LPM cells extending from the trunk. Indeed, the abnormal development of the posterior aortae in *Tgfbr1* mutant embryos might result from compromised development of the *Foxf1*-positive posterior PS/allantois.

To assess whether the PS contributes to the prospective pericloacal region, we generated a transgenic line (*T-str-creERT*) expressing the tamoxifen-inducible cre recombinase in the PS under the control of an enhancer of *Brachyury* (currently known as *Tbxt*)(Clements et al., 1996) and inducing cre-mediated ROSA26-derived reporter expression (Soriano, 1999; Srinivas et al., 2001) (Supplementary Fig. 1). Tamoxifen administration at E8.0, which activates cre activity within the 10-12 hours corresponding to E8.5 (Supplementary Fig. 2), thus coincident with the start of the trunk to tail transition, resulted in labeling of the VLM of E9.5 embryos, and of the pericloacal mesoderm at E10.0 (Fig. 3c). Although this experiment does not allow regional sub localization within the PS, it is consistent with the *Foxf1*-positive posterior PS/allantois being a functional target of *Tgfbr1* activity in the LPM during the trunk to tail transition.

Isl1 mediates *Tgfbr1* activity in the lateral mesoderm

Reporter, gain and loss of function experiments suggested that *Isl1* might be functioning downstream of Tgfbr1 signaling in the LPM during the trunk to tail transition (Dias et al., 2020; Jurberg et al., 2013). It has been shown that *Isl1* first becomes activated in axial tissues at the PS/allantois junction, just prior to the transition to tail development (Cai et al., 2003), and Isl1-positive cells later contribute to the VLM, the hindlimbs and GT (Yang et al., 2006). Analysis of the role of *Isl1* during the trunk to tail transition might thus provide an independent test of the functional relevance of the posterior PS/allantois for *Tgfbr1* activity in the LPM during the transition. We generated *Isl1* null mutant embryos using the null allele resulting from the insertion of the cre recombinase replacing the *Isl1* gene in the *Isl1-cre* strain (Srinivas et al., 2001). *Isl1* null embryos were embryonic lethal between E9.5 and E10.5, showing malformations in different embryonic structures. Regarding axial development, *Isl1* mutants halted their growth around the stage of the trunk to tail transition, as estimated by the number

of somites generated (Fig. 4D,E,F,I,J), thus reminiscent of the *Tgfbr1* mutant phenotype. However, in contrast to *Tgfbr1* mutants, *Isl1* mutants generated a structure resembling the tail bud which expressed *Sox2* and *Tbxt* in domains comparable to wild type embryos (Fig.4A,B,D,E). The presence of a tail bud in *Isl1* mutants indicates that this gene might not be involved in the activity of the NMC cells, as suggested by its expression pattern (Cai et al., 2003). However, we observed major morphological and molecular alterations in the region corresponding to the LPM. Interestingly, some of those alterations are comparable to the defects observed in *Tgfbr1* mutants. The two layers of the lateral mesoderm, as well as the celomic cavity, extended to the posterior extremity of the embryo (Fig. 4H,h',h''). *Foxf1* expression was also upregulated in the posterior of the embryo, showing a spatial distribution that starts at the dorsal border between the splanchnic and somatic LPM layers, extending to fully cover the somatic lateral mesoderm at more posterior embryonic regions (Fig. 4h',h''). In addition, the dorsal aortae were expanded into two globular vessels on either side of the gut tube reaching the caudal embryonic end where they merged ventrally (Figs 4h,h', 5C,c,D,d). The connection between umbilical artery and the expanded DAs was highly disorganized (Fig. 5D). Together, these observations indicate that *Isl1* acts downstream of *Tgfbr1* to regulate the processes associated with the trunk to tail transition in the LPM, including the main vascular system, and are consistent with the *Foxf1*-positive area of the posterior PS/allantois being a functional target of Tgfbr1 signaling to reorganize the LPM during the trunk to tail transition.

Molecular analyses showed that *Tbx4* was not expressed in the posterior part of *Isl1* mutants (Fig. 4I,I',J,J'), indicating that *Tbx4* is downstream of *Isl1* in the regulatory network controlling the hindlimb/external genitalia, consistent with previous observations using a conditional mutant for *Isl1* (Itou et al., 2012; Kawakami et al., 2011).

Proper development of the embryonic endoderm requires *Tgfbr1*

Analysis of transverse sections of the *Tgfbr1* mutant embryos suggested abnormal morphogenesis of the gut tube. Consistent with this, *Foxa2* expression (Ang et al., 1993) at E9.5 seemed to be up regulated at the posterior end of the *Tgfbr1*$^{-/-}$ mutants, also showing abnormal morphology at the posterior end of the gut tube (Fig. 6A,a,B,b). This abnormal morphology was clearer in mutant embryos immunostained with the epithelial marker Keratin 8 (Runck et al., 2014), where it was observed that

the endodermal tube finished contacting the ventral ectoderm forming a structure reminiscent of the cloacal membrane (Fig. 6C,D). Also, in contrast with what was observed in wild type controls, *Tgfbr1*$^{-/-}$ embryos lacked the endodermal widening characteristic of the developing cloaca and failed to extend the endodermal tube caudal to the cloacal membrane to form the tail gut (Fig. 6C,D). Remarkably, expression of the endodermal marker *Apela* (Hassan et al., 2010) followed abnormal patterns in *Tgfbr1* mutants. Contrary to wild type embryos, in which the tail endodermal tube was strongly positive for *Apela* (Fig. 6E,e,F,f), in the *Tgfbr1* mutants most of the endodermal tube was negative for this marker, its expression being observed only in a few cells in the dorsal part of the gut tube (Fig. E',e',F',f'). Surprisingly, *Apela* positive cells were found mixed with the cells of the expanded LPM (Fig. 6E',F'), suggesting that endodermal progenitors were produced but misrouted, failing to enter the gut tube. Consistently with the endodermal origin of the *Apela* positive cells, we observed Keratin 8 staining scattered within the extended LPM of the mutant embryos (Fig. 6c,d).

It has been shown that the visceral endoderm contributes to the formation of the embryonic gut, with the hindgut being particularly populated by this extraembryonic tissue (Kwon et al., 2008). To understand whether the absence of cloacal and tailgut structures in the *Tgfbr1* mutants resulted from the inability of the posterior visceral endoderm cells to become incorporated into the embryonic definitive endoderm, becoming instead mixed with the mis-patterned LPM cells, we introduced the visceral endoderm reporter *Afp-GFP* transgene (Kwon et al., 2008) into the *Tgfbr1* mutant background. Analysis of E7.5 *Afp-GFP*$^{+/0}$*:Tgfbr1*$^{-/-}$ embryos indicated that the dispersal of visceral endodermal cells was not affected by the absence of *Tgfbr1* (Supplementary Fig. 3). In addition, Afp-GFP positive visceral endoderm cells were observed in the embryonic endoderm of *Tgfbr1* mutant embryos at E8.5, in a distribution comparable to wild type embryos (Fig. 7A,A',B,B'). At later stages of development, however, when embryos engage in tail development, distinct distributions were observed in the wild type and mutant embryos. Both at E9.5 and E10.5, the entire endodermal tube of *Tgfbr1*$^{-/-}$ embryos contained GFP positive cells, also showing the premature end at the ventral surface of the embryo and the absence of further posterior extension to form the tail gut (Fig. 7D-D'',F,F'). Importantly, we did not observe Afp-GFP signal mixed with the extended LPM (Fig. 7F'',F'''). These data thus indicate that the absence of *Tgfbr1* does not affect recruitment of visceral

endodermal cells to the embryonic gut, and that the abnormal *Apela* patterns observed in *Tgfbr1* mutant embryos are unlikely to derive from misrouting of visceral endodermal cells.

Interestingly, while we observed a significant contribution of Afp-GFP-positive visceral endoderm cells to the embryonic endoderm of wild type embryos at E8.5 (Fig. 7A,A'), we could detect just a few cells in the tail gut of E9.5 embryos (Fig. 7C-C'') and virtually none at E10.5 (Fig. 7E,E'). This indicates that, while the visceral endoderm contributes significantly to the embryonic gut up to the region of the cloaca, as previously reported (Kwon et al., 2008), it is likely to play a minor role in the extension of the endodermal tube growing into the tail. The *Apela* expression patterns indicate that this gene is active in the newly generated endodermal tissues, becoming progressively downregulated after they are part of the gut tube (Hassan et al., 2010). The strong *Apela* expression restricted to the posterior portion of the endodermal tube within the developing tail, suggests that the tail gut grows from the addition of cells at the tip of this structure. Interestingly, analysis of the *T-str-creERT:ROSA26-R-gal* reporter activity upon tamoxifen administration at E8.0 showed the presence of β-galactosidase positive cells in the tail gut (Fig. 3d). A similar finding has also been independently reported using a different T-creERT strain (Anderson et al., 2013). Of note, more anterior regions of the gut, were negative for β-galactosidase under these conditions, despite the presence of labeled cells in adjacent mesodermal tissues (Fig. 3c). This suggests that the most caudal region of the gut tube grows through the addition of cells generated from a structure derived from the primitive streak located at the end of the growing tail. Consistent with this hypothesis, we observed an *Apela*-positive structure adjacent to the tip of the gut at the posterior end of the growing tail. A similar structure was observed in embryos immunostained for Keratin 8 (Fig. 8; Supplementary Fig. 4).

We further tested the potential of this Apela and Keratin 8- positive region at the tip of the tailbud to contribute to the gut tube using a DiI-mediated cell tracing approach *ex vivo*. E9.5 embryos injected with DiI that showed no label in the gut tube just after injection were analyzed after 20 hours in culture (Fig. 8E-h' and Supplementary Fig. 4). In the three embryos that filled this criterium, DiI-positive cells were observed in the gut tube epithelium. This observation further supports the existence of a region at the tip of the tailbud able to generate cells that become incorporated into the tail gut.

DISCUSSION

The transition from trunk to tail development involves major tissue reorganization affecting all germ layers. Formation of spinal cord and somitic mesoderm is maintained by the relocation of the neural-mesodermal competent cells from the caudal lateral epiblast CLE in the epiblast into the CNH in the tailbud through an incomplete EMT triggered by the concurrent activity of Tgfbr1 and Snai1 (Cambray and Wilson, 2007; Dias et al., 2020; Henrique et al., 2015; Wilson et al., 2009b; Wymeersch et al., 2021, 2019). The progenitors of the lateral mesoderm, however, undergo a process of terminal differentiation resulting in the formation of the primordia of the hindlimb and of the external genitalia (Jurberg et al., 2013). Genetic analyses indicate that *Tgfbr1* signaling is both necessary and sufficient to activate the mechanisms regulating those terminal differentiation processes, as illustrated by their premature activation in transgenic gain of function experiments (Jurberg et al., 2013) and the absence of early markers for the primordia of the hindlimb or the GT in *Tgfbr1* null mutant embryos (Dias et al., 2020). Our data now show that the requirement of *Tgfbr1* encompasses the development of many other tissues undergoing a morphological and functional reorganization during the trunk to tail transition, including the major vascular system and the embryonic endoderm. These observations place *Tgfbr1* as a master regulator of the trunk to tail transition.

An interesting conclusion from our work is the identification of the posterior PS/allantois as a candidate for the structure mediating the different *Tgfbr1*-dependent processes involving the lateral mesoderm and endoderm during the trunk to tail transition. Cell tracing experiments identified the posterior epiblast/PS as the region providing the cells building the trunk LPM (Wymeersch et al., 2016), being the posterior PS abutting the allantois also involved in organizing the recruitment of visceral endodermal cells to the embryonic gut tube (Rodriguez and Downs, 2017). The transition to tail development entails the fading of the epiblast and PS, as they become replaced by the tail bud as the main driver of axial extension. At this stage, the allantois also leaves its position at the posterior end of the embryo to occupy more anterior and ventral positions while organizing the connection between embryonic and extraembryonic structures (Arora and Papaioannou, 2012; Downs and Rodriguez, 2020). Cell tracing experiments indicate that the posterior epiblast/PS, which lays down the LPM during trunk formation, generates the VLM posterior to the allantois

during the trunk to tail transition (Wymeersch et al., 2016) and that these cells contribute to the primordium of the external genitalia later in development (Tschopp et al., 2014). The involvement of the PS in the formation of the VLM and genital primordia is also supported by our reporter data with the *T-str-creERT* transgenic line and *Isl1* cell lineage analyses (Yang et al., 2006). The absence of VLM in the *Tgfbr1* mutants indicates that signaling through this receptor is required to organize the proper switch of the posterior epiblast/PS from a trunk developmental mode, involving entering VLM fates. *Foxf1*, which is expressed in the posterior PS, maintains expression in the derivatives of this structure after the transition to tail development (Supplementary Fig. 5) (Astorga and Carlsson, 2007). We suggest that the strong and expanded *Foxf1* expression throughout the posterior end of the extended LPM of the *Tgfbr1* mutant embryos represents a molecular vestige of posterior PS that failed to form the VLM, and instead became trapped within mis-patterned LPM extending from the trunk. As the posterior PS is also thought to play a relevant role in the connection of the paired DAs with the allantois artery to link the embryonic and extraembryonic vascular systems (Downs and Rodriguez, 2020), defective posterior PS reorganization during the trunk to tail transition could explain the DA abnormalities observed in the *Tgfbr1* mutant embryos.

The embryonic tailgut has received little attention and mechanisms of its growth remain largely unknown. Analysis of *Tgfbr1*$^{-/-}$ embryos revealed that signaling through this receptor is essential for the development of the endodermal tube posterior to the cloacal plate and potentially the cloaca itself. *Apela* expression in wild type embryos is high in the newly formed endoderm, becoming downregulated as the endodermal tube differentiates (Hassan et al., 2010). The presence of the highest *Apela* levels in the posterior part of the tail gut at different embryonic stages (Hassan et al., 2010) suggests that this structure grows through the addition of new tissue at its posterior end. The low levels of *Apela* expression in the endoderm of the *Tgfbr1* mutants might thus indicate that this structure was generated earlier in development, during the phase of trunk extension. In addition, the presence of *Apela* signal mixed with the LPM suggests that new endodermal cells are still produced but failed to enter the gut, being instead mistargeted to the mesoderm. The absence of fluorescence signal in the mesodermal tissue of *Tgfbr1*$^{-/-}$*:Afp-GFP* embryos indicates that those cells are most likely not derived from the posterior visceral endoderm (Kwon et al., 2008). Interestingly, the similarities between the *Apela* and *Foxf1* expression in the posterior

region of *Tgfbr1* mutant embryos suggest that their developmental history might be somehow linked. Given the role of the posterior PS abutting the allantois in the recruitment of visceral endodermal cells to the embryonic gut (Rodriguez and Downs, 2017), it is possible that tail gut growth is organized by a structure derived from a specific region of the posterior PS that enters the tail during the transition to tail development. The existence of a region at the tip of the tailbud that feeds cells to the gut tube is supported by our DiI tracing experiment. In addition, the observation that the ROSA26 reporter labels the gut tail when activated by the *T-str-creERT* driver at the stage of the trunk to tail transition (Anderson et al., 2013) (Fig. 3d) is consistent with the involvement of the PS or a derivative of this structure in the formation of the gut tube posterior to the cloacal membrane. Were this the case, the transition of this PS-derived structure should be under *Tgfbr1* control.

Taken together, this work along with previous studies, suggests that the control of the trunk to tail transition by *Tgfbr1* entails two distinct, and apparently independent, components acting on two areas of the epiblast/PS. The first component involves a cooperation between *Tgfbr1* and *Snai1* to organize the relocation of NMC progenitors from the CLE to the CNH through a partial EMT (Dias et al., 2020). This component is also associated with the generation of the tail bud that replaces the epiblast/PS as the driver of axial elongation (Wilson et al., 2009b; Wymeersch et al., 2021). The second component would target the posterior part of the epiblast/PS containing the progenitors for the lateral mesoderm as well as an organizing center for endodermal development (summarized in Fig. 9). Here, *Tgfbr1* activity triggers a combination of programs leading to the organization of the exit channels of the intestinal and urogenital systems, as well as the connection of the embryonic and extraembryonic circulation, and the formation of the hindlimbs and external genitalia. The finding that *Isl1* mutants exhibit many of the features observed in the lateral mesoderm and vascular system of *Tgfbr1* mutants, together with the absence of *Isl1* expression in *Tgfbr1* mutants identifies *Isl1* as a key downstream mediator of the second component of *Tgfbr1* activity controlling the trunk to tail transition. Additional work will be required to elucidate the mechanisms regulating the fate and cell dynamics of the posterior epiblast/PS during the trunk to tail transition.

ACKNOWLEDGEMENTS

We would like to thank the members of the Mallo lab, especially Ana Casaca for continuous support at different stages of this project and the IGC mouse facility for their help with animal housing, and the Mouse Genetics Core Facility of Memorial Sloan Kettering Cancer Center for rederivation of the *Tgfbr1* mouse line.

FUNDING

This project was funded by Fundação para a Ciência e a Tecnologia (FCT) grants 2022.01629.PTDC to MM, the PhD fellowship PD/BD/128437/2017 to AL and the research infrastructure Congento LISBOA-01-0145-FEDER-022170 to the animal facility, co-financed by Lisboa 2020/FEDER and FCT (Portugal). AKH and YYK are supported by the NIH (R01DK127821, R01HD094868, R01HD035455, and P30CA008748).

REFERENCES

Aires R, de Lemos L, Nóvoa A, Jurberg AD, Mascrez B, Duboule D, Mallo M. 2019. Tail Bud Progenitor Activity Relies on a Network Comprising Gdf11, Lin28, and Hox13 Genes. *Dev Cell* **48**:383–395. doi:10.1016/j.devcel.2018.12.004

Anderson MJ, Naiche LA, Wilson CP, Elder C, Swing DA, Lewandoski M. 2013. TCreERT2, a Transgenic Mouse Line for Temporal Control of Cre-Mediated Recombination in Lineages Emerging from the Primitive Streak or Tail Bud. *PLoS One* **8**:e62479. doi:10.1371/journal.pone.0062479

Andersson O, Reissmann E, Ibáñez CF. 2006. Growth differentiation factor 11 signals through the transforming growth factor-beta receptor ALK5 to regionalize the anterior-posterior axis. *EMBO Rep* **7**:831–837. doi:10.1038/sj.embor.7400752

Ang S-L, Wierda A, Wong D, Stevens KA, Cascio S, Rossant J, Zaret KS. 1993. The formation and maintenance of the definitive endoderm lineage in the mouse: involvement of HNF3/forkhead proteins. *Development* **119**:1301–1315.

Arora R, Papaioannou VE. 2012. The murine allantois: A model system for the study of blood vessel formation. *Blood*. doi:10.1182/blood-2012-03-390070

Astorga J, Carlsson P. 2007. Hedgehog induction of murine vasculogenesis is mediated by Foxf1 and Bmp4. *Development* **134**:3753–3761. doi:10.1242/dev.004432

Binagui-Casas A, Dias A, Guillot C, Metzis V, Saunders D. 2021. Building consensus in neuromesodermal research: Current advances and future biomedical perspectives. *Curr Opin Cell Biol* **73**:133–140. doi:10.1016/j.ceb.2021.08.003

Cai C-L, Liang X, Shi Y, Chu P-H, Pfaff SL, Chen J, Evans S. 2003. Isl1 Identifies a Cardiac Progenitor Population that Proliferates Prior to Differentiation and Contributes a Majority of Cells to the Heart Expression of Fgf10 and the Fgf10-lacZ transgene in, Developmental Cell.

Cambray N, Wilson V. 2007. Two distinct sources for a population of maturing axial progenitors. *Development* **134**:2829–2840. doi:10.1242/dev.02877

Clements D, Taylor HC, Herrmann BG, Stott D. 1996. Distinct regulatory control of the Brachyury gene in axial and non-axial mesoderm suggests separation of mesoderm lineages early in mouse gastrulation. *Mech Dev* **56**:139–149.

Cohn MJ. 2011. Development of the external genitalia: Conserved and divergent mechanisms of appendage patterning. *Developmental Dynamics* **240**:1108–1115. doi:10.1002/dvdy.22631

Dias A, Lozovska A, Wymeersch FJ, Nóvoa A, Binagui-Casas A, Sobral D, Martins GG, Wilson V, Mallo M. 2020. A Tgfbr1/Snai1-dependent developmental module at the core of vertebrate axial elongation. *Elife* **9**:e56615. doi:10.7554/eLife.56615

Downs KM, Rodriguez AM. 2020. The mouse fetal-placental arterial connection: A paradigm involving the primitive streak and visceral endoderm with implications for human development. *Wiley Interdiscip Rev Dev Biol*. doi:10.1002/wdev.362

Funayama N, Sato Y, Matsumoto K, Ogura T, Takahashi Y. 1999. Coelom formation: binary decision of the lateral plate mesoderm is controlled by the ectoderm. *Development* **126**:4129–4138.

Hassan AS, Hou J, Wei W, Hoodless PA. 2010. Expression of two novel transcripts in the mouse definitive endoderm. *Gene Expression Patterns* **10**:127–134. doi:10.1016/j.gep.2010.02.001

Henrique D, Abranches E, Verrier L, Storey KG. 2015. Neuromesodermal progenitors and the making of the spinal cord. *Development* **142**:2864–2875. doi:10.1242/dev.119768

Hogan B, Beddington R, Constantini F, Lacy E. 1994. Manipulating the mouse embryo: a laboratory manual, 2nd ed. Cold Spring Harbour Laboratory Press.

Huang YC, Chen F, Li X. 2016. Clarification of mammalian cloacal morphogenesis using high-resolution episcopic microscopy. *Dev Biol* **409**:106–113. doi:10.1016/j.ydbio.2015.10.018

Itou J, Kawakami H, Quach T, Osterwalder M, Evans SM, Zeller R, Kawakami Y. 2012. Islet1 regulates establishment of the posterior hindlimb field upstream of the Hand2-Shh morphoregulatory gene network in mouse embryos. *Development* **139**:1620–1629. doi:10.1242/dev.073056

Jurberg AD, Aires R, Varela-Lasheras I, Nóvoa A, Mallo M. 2013. Switching axial progenitors from producing trunk to tail tissues in vertebrate embryos. *Dev Cell* **25**:451–462. doi:10.1016/j.devcel.2013.05.009

Kawakami Y, Marti M, Kawakami H, Itou J, Quach T, Johnson a., Sahara S, O'Leary DDM, Nakagawa Y, Lewandoski M, Pfaff S, Evans SM, Belmonte JCI. 2011. Islet1-mediated activation of the -catenin pathway is necessary for hindlimb initiation in mice. *Development* **138**:4465–4473. doi:10.1242/dev.065359

Kwon GS, Viotti M, Hadjantonakis AK. 2008. The Endoderm of the Mouse Embryo Arises by Dynamic Widespread Intercalation of Embryonic and Extraembryonic Lineages. *Dev Cell* **15**:509–520. doi:10.1016/j.devcel.2008.07.017

Mahlapuu M, Ormestad M, Enerbäck S, Carlsson P. 2001. The forkhead transcription factor Foxf1 is required for differentiation of extra-embryonic and lateral plate mesoderm. *Development* **128**:155–166.

Matsubara Y, Hirasawa T, Egawa S, Hattori A, Suganuma T, Kohara Y, Nagai T, Tamura K, Kuratani S, Kuroiwa A, Suzuki T. 2017. Anatomical integration of the sacral-hindlimb unit coordinated by GDF11 underlies variation in hindlimb positioning in tetrapods. *Nat Ecol Evol* **1**:1392–1399. doi:10.1038/s41559-017-0247-y

Matsumaru D, Murashima A, Fukushima J, Senda S, Matsushita S, Nakagata N, Miyajima M, Yamada G. 2015. Systematic stereoscopic analyses for cloacal development: The origin of anorectal malformations. *Sci Rep* **5**:13943. doi:10.1038/srep13943

McPherron AC, Huynh T V, Lee S-J. 2009. Redundancy of myostatin and growth/differentiation factor 11 function. *BMC Dev Biol* **9**:24. doi:10.1186/1471-213X-9-24

McPherron AC, Lawle AM, Lee S-J. 1999. Regulation of anterior/posterior patterning of the axial skeleton by growth/differentiation factor 11. *Nat Genet* **22**:260–264. doi:10.1038/10320
Nowotschin S, Hadjantonakis AK, Campbell K. 2019. The endoderm: A divergent cell lineage with many commonalities. *Development (Cambridge)*. doi:10.1242/dev.150920
Prummel KD, Nieuwenhuize S, Mosimann C. 2020. The lateral plate mesoderm. *Development (Cambridge)* **147**:dev175059. doi:10.1242/dev.175059
Renier N, Wu Z, Simon DJ, Yang J, Ariel P, Tessier-Lavigne M. 2014. IDISCO: A simple, rapid method to immunolabel large tissue samples for volume imaging. *Cell* **159**:896–910. doi:10.1016/j.cell.2014.10.010
Rodriguez AM, Downs KM. 2017. Visceral endoderm and the primitive streak interact to build the fetal-placental interface of the mouse gastrula. *Dev Biol* **432**:98–124. doi:10.1016/j.ydbio.2017.08.026
Runck LA, Method A, Bischoff A, Levitt M, Penã A, Collins MH, Gupta A, Shanmukhappa S, Wells JM, Guasch G. 2014. Defining the molecular pathologies in cloaca malformation: Similarities between mouse and human. *DMM Disease Models and Mechanisms* **7**:483–493. doi:10.1242/dmm.014530
Soriano P. 1999. Generalized lacZ expression with the ROSA26 Cre reporter strain. *Nat Genet* **21**:70–71. doi:10.1038/5007
Srinivas S, Watanabe T, Lin C-S, William CM, Tanabe Y, Jessell TM, Costantini F. 2001. Cre reporter strains produced by targeted insertion of EYFP and ECFP into the ROSA26 locus. *BMC Dev Biol* **1**:4. doi:10.1186/1471-213X-1-4
Steventon B, Martinez Arias A. 2017. Evo-engineering and the cellular and molecular origins of the vertebrate spinal cord. *Dev Biol* **432**:3–13. doi:10.1016/j.ydbio.2017.01.021
Tickle C. 2015. How the embryo makes a limb: Determination, polarity and identity. *J Anat* **227**:418–430. doi:10.1111/joa.12361
Tsakiridis A, Wilson V. 2015. Assessing the bipotency of in vitro-derived neuromesodermal progenitors. *F1000Res* **4**:100. doi:10.12688/f1000research.6345.2
Tschopp P, Sherratt E, Sanger TJ, Groner AC, Ariel C, Hu JK, Pourquié O, Gros J, Tabin CJ. 2014. A relative shift in cloacal location repositions external genitalia in amniote evolution. *Nature* **516**:391–394. doi:10.1038/nature13819.A
Tsiairis CD, McMahon AP. 2009. An Hh-Dependent Pathway in Lateral Plate Mesoderm Enables the Generation of Left/Right Asymmetry. *Current Biology* **19**:1912–1917. doi:10.1016/j.cub.2009.09.057
Wilson V, Olivera-Martínez I, Storey KG. 2009a. Stem cells, signals and vertebrate body axis extension. *Development* **136**:1591–1604. doi:10.1242/dev.039172
Wilson V, Olivera-Martinez I, Storey KG. 2009b. Stem cells, signals and vertebrate body axis extension. *Development* **136**:2133–2133. doi:10.1242/dev.039172
Wymeersch FJ, Huang Y, Blin G, Cambray N, Wilkie R, Wong FCK, Wilson V. 2016. Position-dependent plasticity of distinct progenitor types in the primitive streak. *Elife* **5**:e10042. doi:10.7554/eLife.10042
Wymeersch FJ, Skylaki S, Huang Y, Watson JA, Economou C, Marek-Johnston C, Tomlinson SR, Wilson V. 2019. Transcriptionally dynamic progenitor populations organised around a stable niche drive axial patterning. *Development* **146**:dev168161. doi:10.1242/dev.168161
Wymeersch FJ, Wilson V, Tsakiridis A. 2021. Understanding axial progenitor biology in vivo and in vitro. *Development* **148**:dev180612. doi:10.1242/dev.180612
Yamada G, Suzuki K, Haraguchi R, Miyagawa S, Satoh Y, Kamimura M, Nakagata N, Kataoka H, Kuroiwa A, Chen Y. 2006. Molecular genetic cascades for external genitalia

formation: An emerging organogenesis program. *Developmental Dynamics* **235**:1738–1752. doi:10.1002/dvdy.20807

Yang L, Cai CL, Lin L, Qyang Y, Chung C, Monteiro RM, Mummery CL, Fishman GI, Cogen A, Evans S. 2006. Isl1 Cre reveals a common Bmp pathway in heart and limb development. *Development* **133**:1575–1585. doi:10.1242/dev.02322

Zakin L, Reversade B, Kuroda H, Lyons K, De Robertis E. 2005. Sirenomelia in Bmp7 and Tsg compound mutant mice: requirement for Bmp signaling in the development of ventral posterior mesoderm. *Development* **132**:2489–2499. doi:dev.01822 [pii]\n10.1242/dev.01822

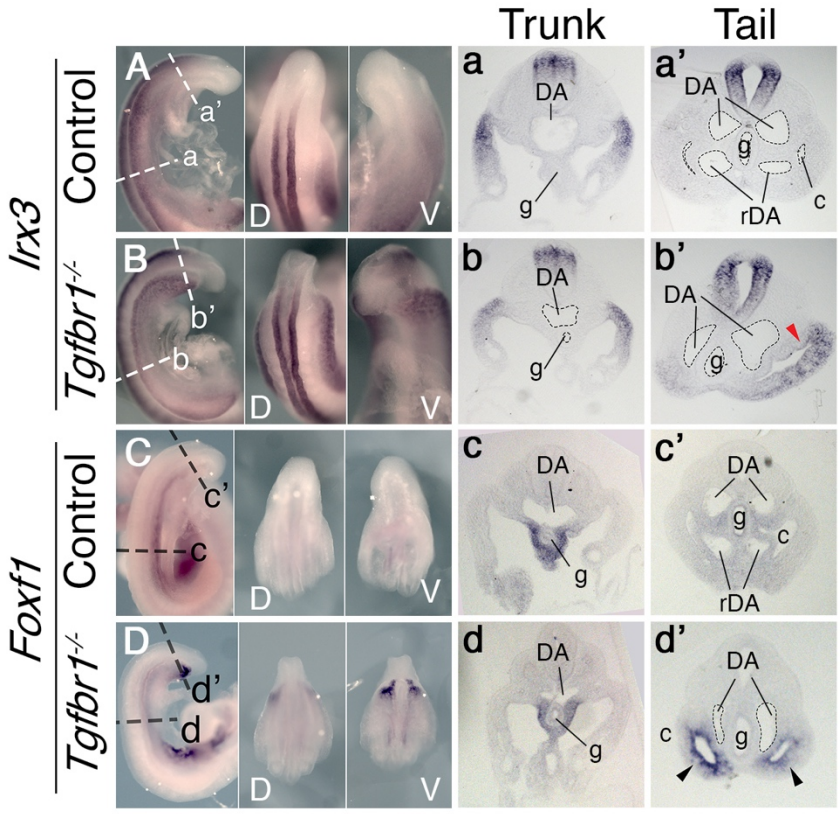

Figure 1. In situ hybridization showing expression patterns of the main mesodermal markers. A – d'. Expression of somatic LPM marker *Irx3* (A, B) and splanchnic LPM marker *Foxf1* (C, D) in control (A, C) and *Tgfbr1*$^{-/-}$ (B, D) E9.5 embryos. Next to the images of the whole mount embryos shown transversal sections through trunk (a – d) and tail (a' – d') regions. Red arrowhead indicates ectopic expression of *Irx3* in splanchnic LPM, black arrowhead – ectopic expression of *Foxf1* in somatic LPM. c – coelomic cavity, cl – cloaca, DA – dorsal aorta, g – gut, g – gut, rDA – recurved dorsal aorta, V – ventral, D – dorsal.

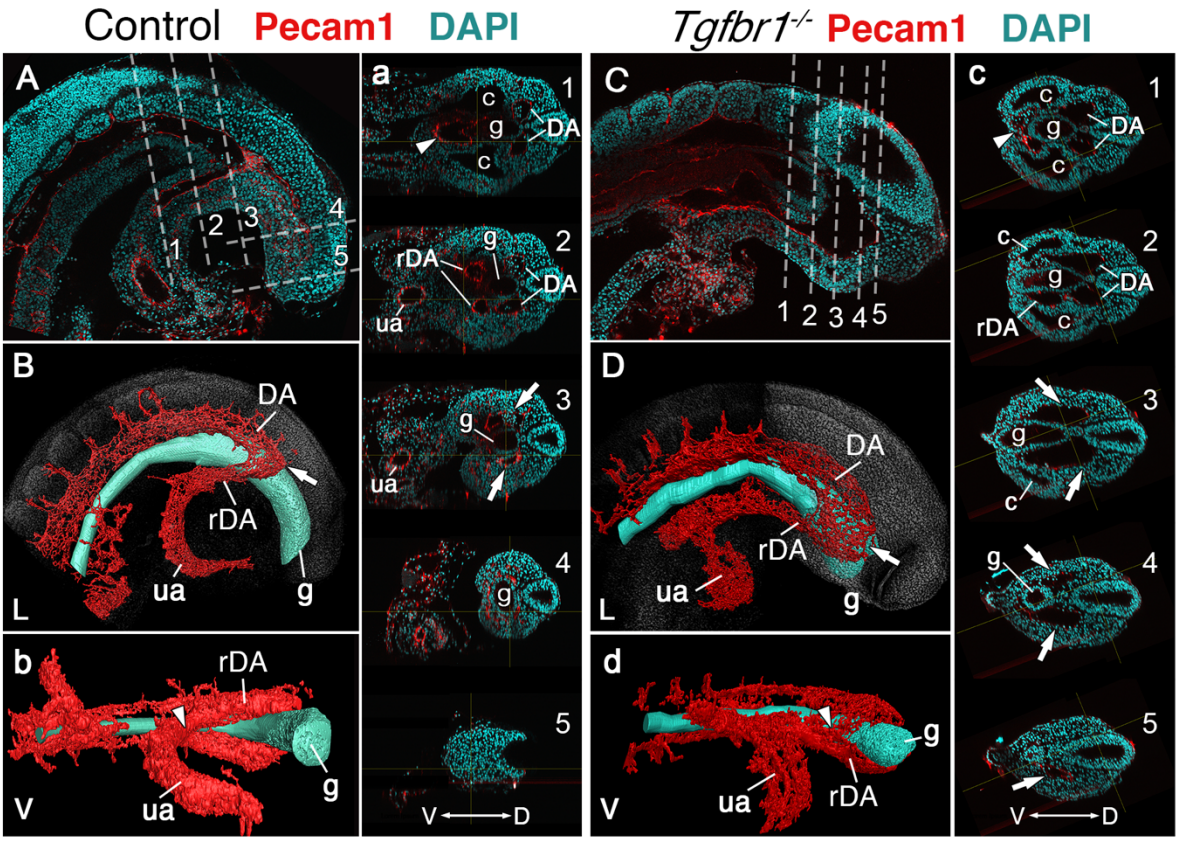

Figure 2. Main vascular tree of the *Tgfr1*$^{-/-}$ embryos. A, a, C, c. Wholemount immunostaining for Pecam1 (red) labelling endothelial cells in E9.5 control (A, a) and mutant (C, c) embryos. Nuclei shown in cyan. Transversal sections through regions marked by the dashed lines in A and C are shown in (a1-5) and (c1-5). **B, b, D, d.** 3D reconstruction of the main vascular tree (red) and the gut (cyan) of the immunostaining shown in (A, a, C, c). Connection between the umbilical artery (ua) and recurved dorsal aortae (rDA) is marked by the arrowhead. Turn of dorsal aortae (DA) where it is connected to rDA is labelled by the arrow. In the mutant this region is enlarged while rDA is short (compare A, a3 and B to C, c2-5, and D). D – dorsal, L – lateral, V – ventral, c – coelomic cavity, g – gut.

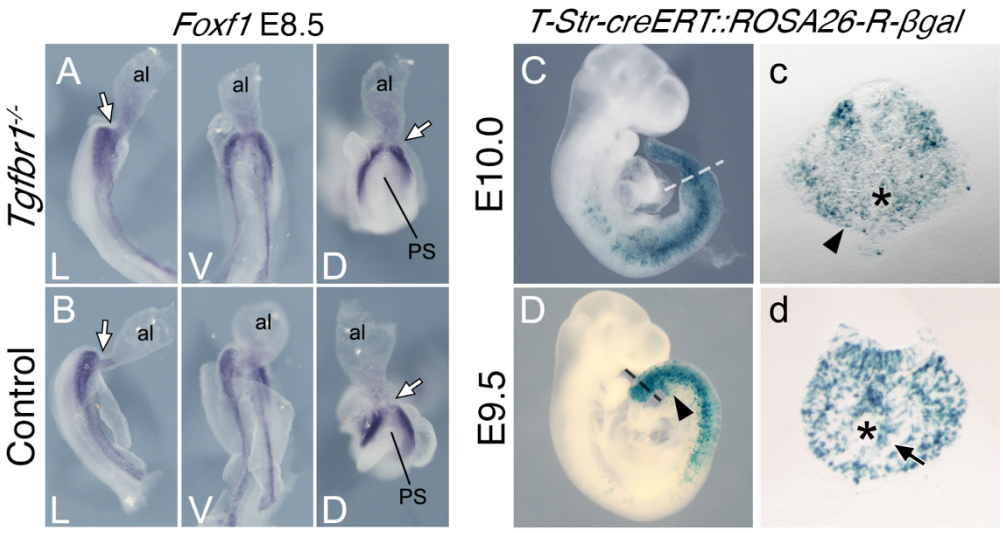

Figure 3. Posterior primitive streak contributes to the pericloacal mesenchyme and gut endoderm. A, B. Whole mount in situ hybridization showing expression of *Foxf1* in E8.5 *Tgfbr1*$^{-/-}$ (A) and control (B) embryos. al – allantois, g – gut, PS – primitive streak. L – lateral view, V – ventral view, D – dorsal view. While arrow indicates PS/allantois junction. **C-d.** β-galactosidase cell tracing showing descendance of the primitive streak in the E10.0 (C, c) and E9.5 (D, d) embryos. c and d show transversal sections through regions marked by the dashed lines in C and D. Black arrowhead shows β-galactosidase staining in the pericloacal mesenchyme. Black arrow in d shows β-galactosidase^{+} cells in the tail gut endoderm. The asterisk in c indicates the cloaca. The asterisk in d indicates the tail gut.

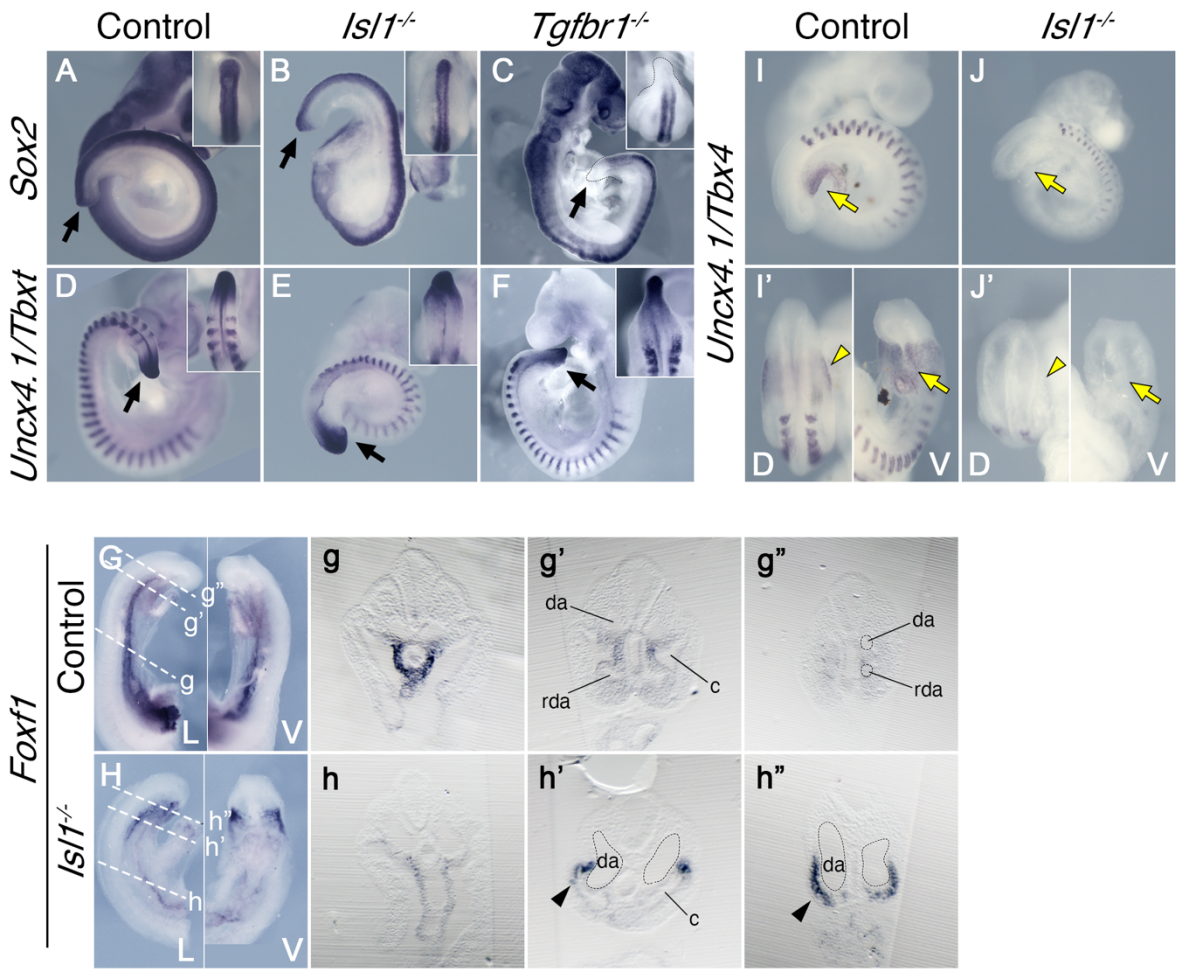

Figure 4. Effects of *Tgfbr1* in the LPM, but not in the tail bud, are mediated by *Isl1*. A-F". Whole mount *in situ* hybridization showing expression of *Sox2* (A-C) and *Uncx4.1/Tbxt* (D-F) in the E9.5 control (A, D), *Isl1*$^{-/-}$ (B, E), and *Tgfbr1*$^{-/-}$ (C, F) embryos. *Isl1*$^{-/-}$ embryos form tail bud (black arrows), unlike *Tgfbr1*$^{-/-}$ embryos. Insets in the right top corners show dorsal view of the tail bud region. **G, h".** Whole mount *in situ* hybridization showing expression of *Foxf1* in the E9.5 control (G) and *Isl1*$^{-/-}$ (H) embryos. g-g" and h-h" show transversal sections through the regions marked by the dashed line in G and H. *Foxf1* is ectopically expressed in the splanchnopleure of the posterior region of the *Isl1*$^{-/-}$ (black arrowhead in h' and h"). **I-J'.** Whole mount *in situ* hybridization showing expression of *Uncx4.1/Tbx4* in E9,5 control (I, I') and *Isl1*$^{-/-}$ (J, J') embryos. *Tbx4* is not expressed in pericloacal mesenchyme (yellow arow) and hindlimb buds (yellow arrowheads) of *Isl1*$^{-/-}$ mutants. da – dorsal aorta, rda – recurved dorsal aorta, c – coelomic cavity, D – dorsal, V – ventral.

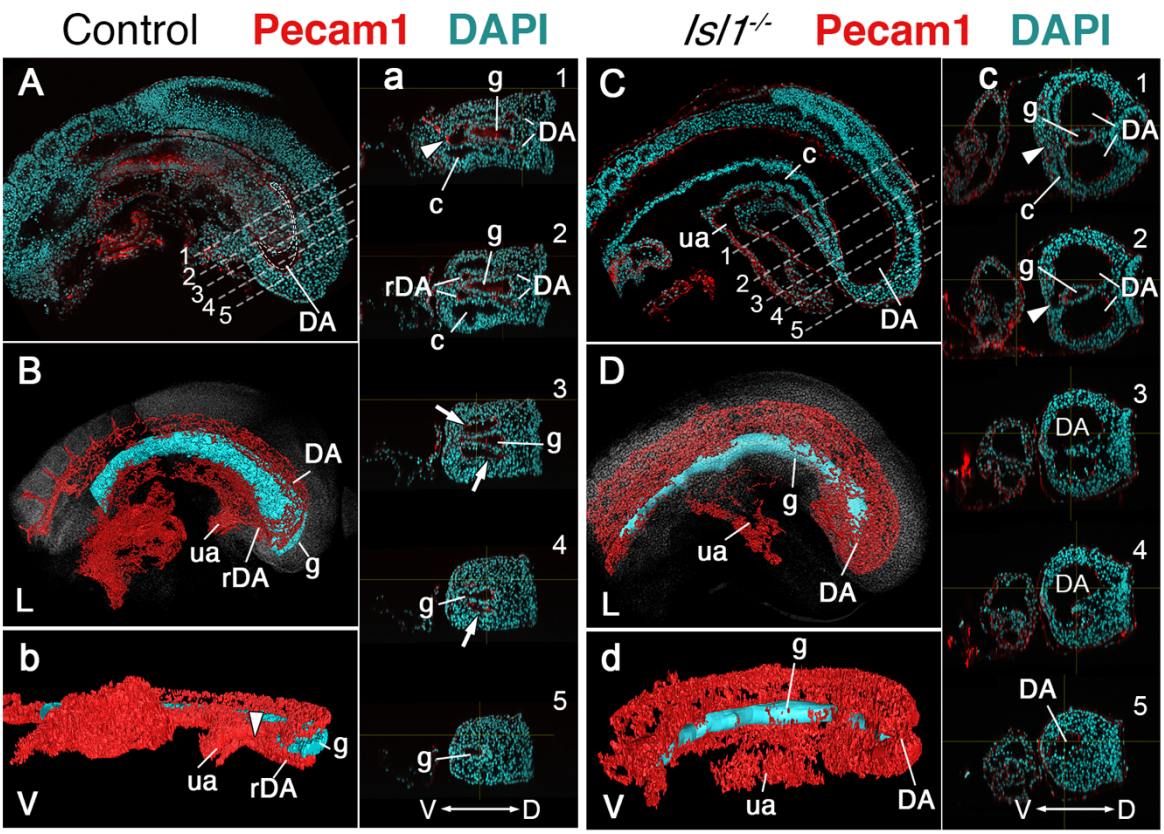

Figure 5. Main vascular tree of the *Isl1*$^{-/-}$ embryos. A, C. Wholemount immunostaining for Pecam1 (red) labelling endothelial cells in E9.5 control (A) and mutant (C) embryos. **a, c.** Optical transversal sections through regions marked by the dashed lines in A and C. **B, b, D, d.** 3D reconstruction of the main vascular tree (red) and the gut (cyan) of the immunostaining shown in (A, a, C, c). In the mutant recurved dorsal aorta (rDA) is underdeveloped and connection between dorsal aortae (DA) and the umbilical artery (ua) is established by a small vessel (white arrowhead in c1 and c2). Branches of DA are enlarged in the *Isl1*$^{-/-}$ and merge together at the posterior end and ventral to the gut (c3-5, d). D – dorsal, L – lateral, V – ventral, c – coelomic cavity, g – gut.

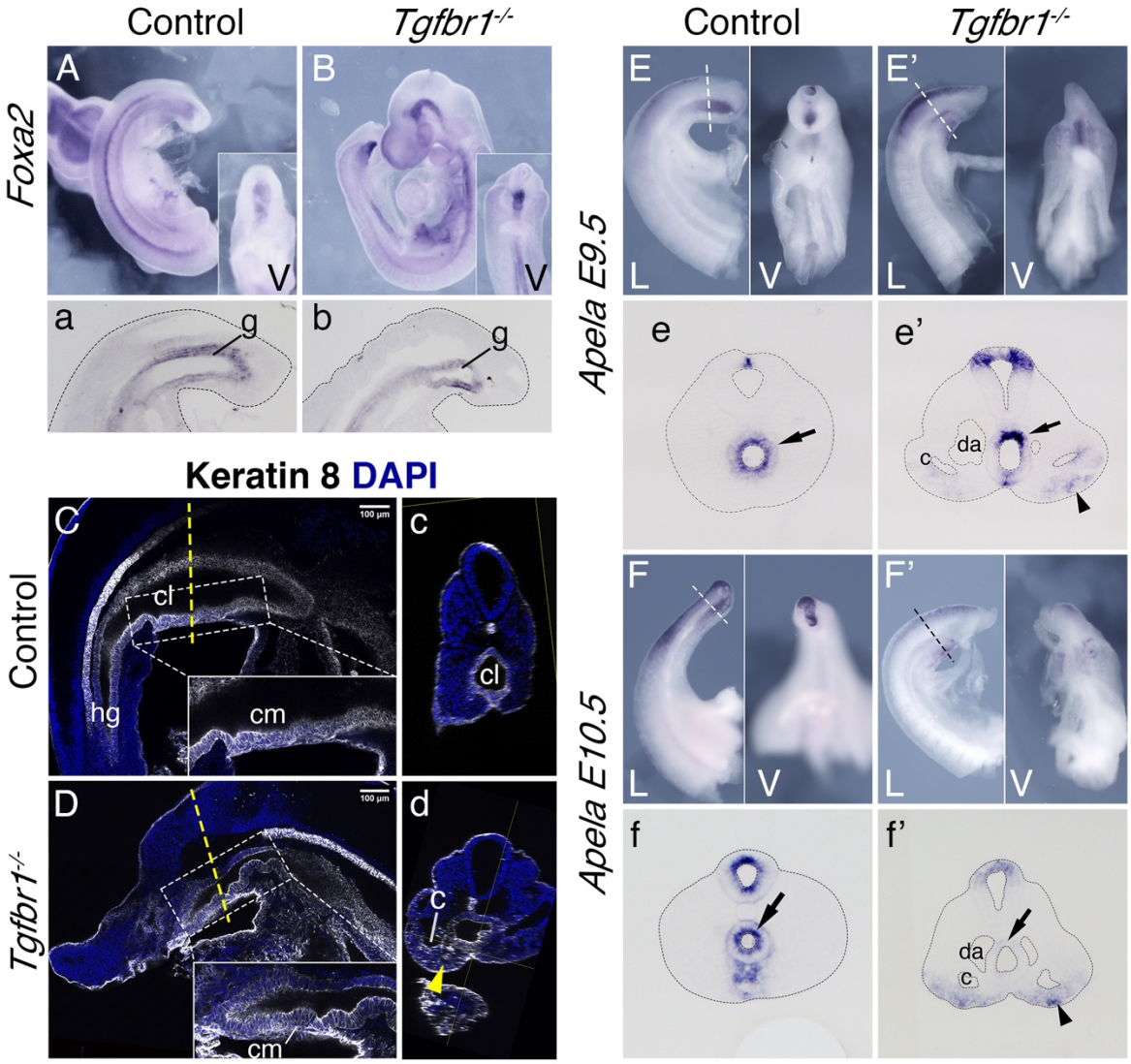

Figure 6. Endoderm of the *Tgfbr1* KO. A – b. Expression of *Foxa2* in E9.5 control (A, a) and *Tgfbr1* KO (B, b) embryos. a, b. show sagittal sections though the tail region. **C - d.** Keratin 8 staining of the cloaca region in the control (C,c) and *Tgfbr1*$^{-/-}$ (D,d) E10.5 embryos. *Tgfbr1*$^{-/-}$ do not initiate enlargement of the cloacal cavity. Insets show higher magnification of the cloacal membrane (cm). c and d show transversal optical sections marked by the dashed line in C and D. Yellow arrowhead in d shows keratin 8 staining in expanded LPM of the *Tgfbr1* mutant embryo. **E – e'.** *Apela* expression in the posterior region of the E9.5 control (E, e) and mutant (E', e') embryos. e and e' show transversal sections of regions marked by the dashed line in E and E'. **F–f'.** *Apela* expression in the posterior region of the E10.5 control (F, f) and mutant (F', f') embryos. f and f' show transversal sections of regions marked by the dashed line in F and F'. Black arrow – gut endoderm, black arrowhead – *Apela*-expressing cells in LPM of the mutant embryo. V–ventral, L–lateral, cl – cloaca, c – coelomic cavity, da – dorsal aorta, g – gut, hg – hindgut.

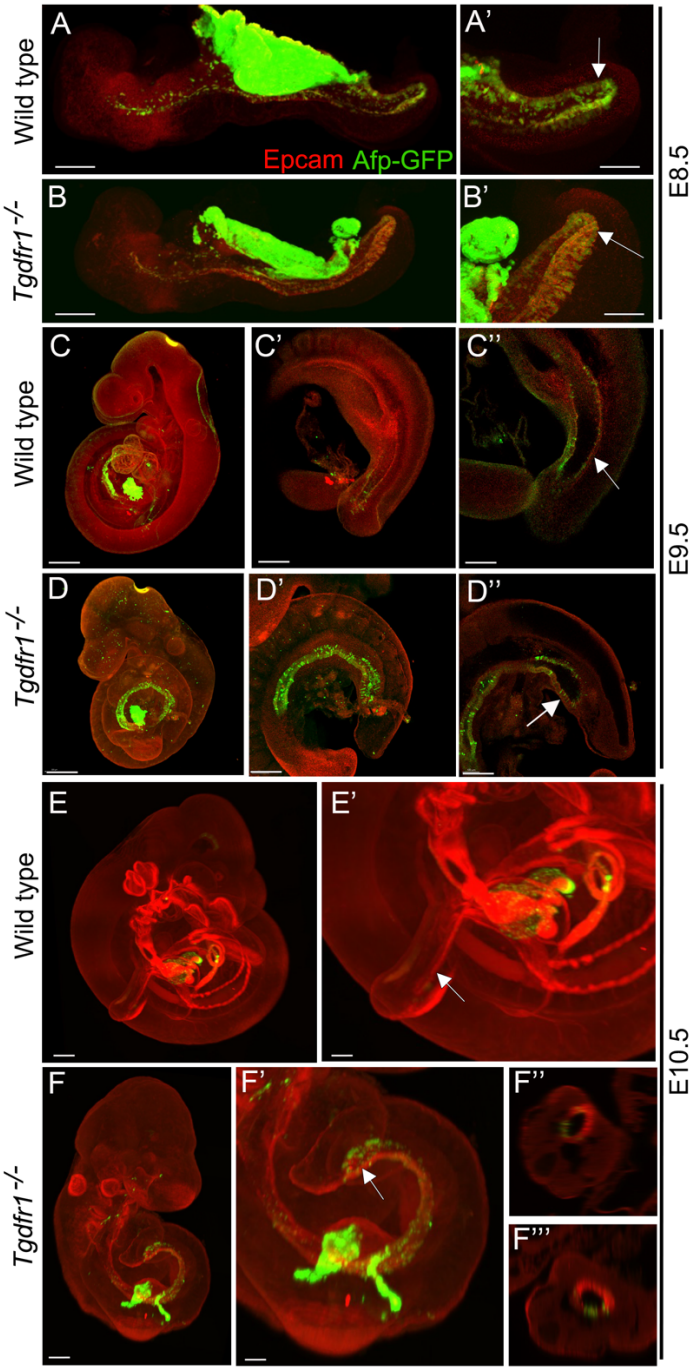

Figure 7. Analysis of the contribution of the visceral endoderm to the embryonic gut. GFP expression from the Afp-GFP transgenics was analyzed at E8.5 (A-B'), E9.5 (C-D'') or E10.5 (E-F''') in wild type (A, A', C-C'', E,E') or *Tgfbr1*$^{-/-}$ (B, B',D-D'', F-F''') embryos. C' and D' show a 3D image of the embryo, and C'' and D'' show transversal sections. F' and F'' show transversal sections through the caudal part of F'. The embryonic endoderm was labeled by immunofluorescence against Epcam. Arrows in A', B' indicate the hindgut; arrows in C'' and E' indicate the tail gut; arrows in D'' and F' indicate the cloacal membrane. Size bars: A, B: 200 μm; A', B': 100 μm; C, D: 300 μm; C', D': 200 μm; C'', D'': 150 μm; E: 300 μm; F: 200 μm; E': 150 μm; F': 100 μm.

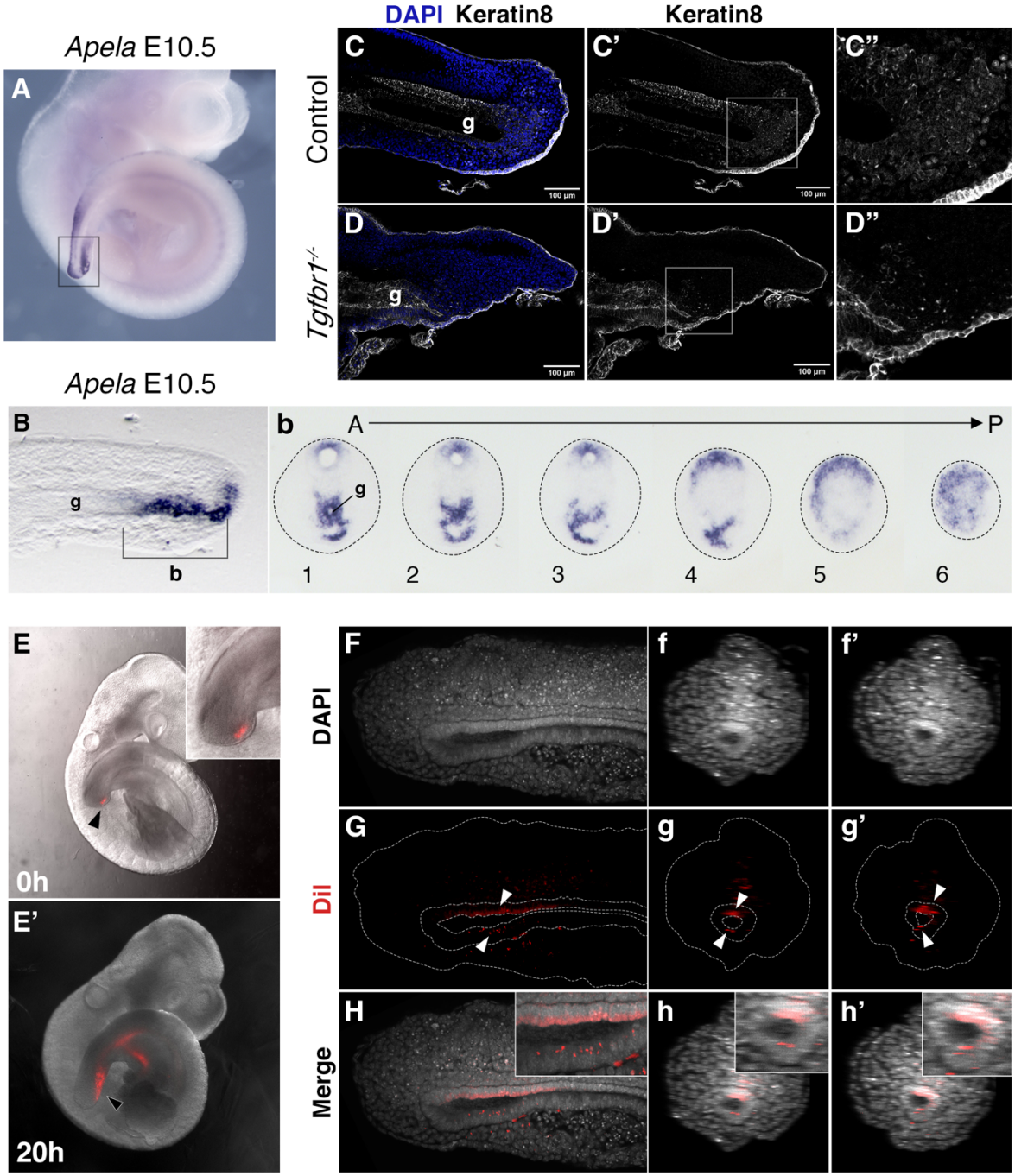

Figure 8. Tail gut endoderm have contribution from the posterior pool of tailbud cells. A. Whole mount *in situ* hybridization showing expression of *Apela* in E10.5 wild type embryo. **B.** Sagittal section through the region marked by rectangle in A shows presence of *Apela*-stained structure posterior to tail gut endoderm. **b.** Series of transversal sections though the *Apela*-expressing region posterior to the gut endoderm (marked by square bracket in B). **C-D".** Sagittal optical sections through the tail region of the whole-mount immunostaining for Keratin 8 (white) in E10.5 control (C-C") and *Tgfbr1*$^{-/-}$ (D-D") embryos. Nuclei are shown in blue. Squares in C' and D' show the pool of epithelial cells posterior to the tail gut tube. This region coincides with newly formed endodermal cells expressing *Apela* shown in B, b. C". D" higher magnification of the region marked by square in C' and D'. A – anterior, P – posterior, g – gut. **E, E'**. Whole mount images of embryos injected with DiI in the Apela-positive region of the tail bud posterior to the gut endoderm, just after injection (E) or after 20 hours of

incubation (E'). The magnification of the tail bud in the inset shows the absence of label in the gut tube. **F-h'.** Optical sections from two-photon images of the embryo in E' to show the presence of DiI cells in the gut tube. F-H show sagittal sections; f-h' show transverse sections. F-f' show the DAPI channel, G-g' shows the DiI channel, highlighting the gut structures with a dotted line and the presence of DiI positive cells within the gut with arrowheads, and H-h' shows a merge of both channels.

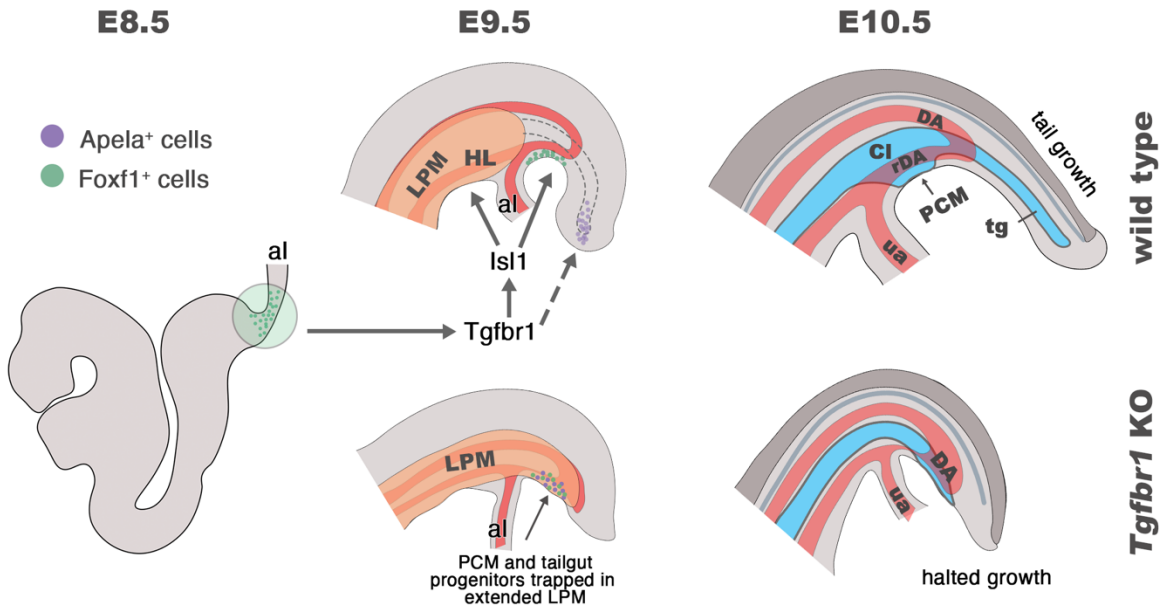

Figure 9. Schematic representation of *Tgfbr1* activity on the posterior epiblast/PS region during the trunk to tail transition. At E8.5 embryo undergoes turning, associated with anterior relocation of the allantois along the ventral side of the embryo. In wild type embryos (top panel) *Tgfbr1* acts upstream of *Isl1*, which induces hindlimb (HL) formation from the somatic LPM, marking the posterior limit of this mesodermal compartment. Additionally, *Isl1* is involved in formation of the pericloacal mesenchyme (PCM), likely from the *Foxf1*$^+$ region in the posterior PS (shown in green), and in the development of the recurved dorsal aorta (rDA). Tailgut (tg) growth is, at least in part, supplied by the cells located in the tail bud (endodermal Apela$^+$ cells are shown in purple). At E10.5 the trunk to tail transition is completed, resulting in the formation of the posterior trunk structures, including HL, cloaca (Cl), PCM and the connection of embryonic/extraembryonic (umbilical artery - ua) blood circulation via rDA. Tail growth continues generating neural tube (dark grey), presomitic mesoderm (not shown), and tg (blue). In the absence of *Tgfbr1* (bottom panel) *Isl1* is not activated, hindlimbs are not induced from the LPM, which, instead, keeps extending posteriorly. PCM and tg progenitor cells are misrouted and trapped in the posteriorly extended LPM. The rDA is underdeveloped. Development of *Tgfbr1* mutants is halted around E10.5.

Table 1

Genotyping primers		
Tgfbr1 mutant allele	Forward	CTACTGTGTTTCAAATGGGAGGGC
	Reverse	GGCCTGTCGGATCCTATCATC
Tgfbr1 wild type allele	Forward	CTACTGTGTTTCAAATGGGAGGGC
	Reverse	ACATACAAATGGCCTGTCTCG
Isl1 mutant allele	Forward	GCCACTATTTGCCACCTAGC
	Reverse	AGGCAAATTTTGGTGTACGG
Isl1 wild type allele	Forward	GCCACTATTTGCCACCTAGC
	Reverse	CAAATCCAAAGAGCCCTGTC
Cre recombinase	Forward	CGAGTGATGAGGTTCGCAAG
	Reverse	CCTGATCCTGGCAATTTCGGCT

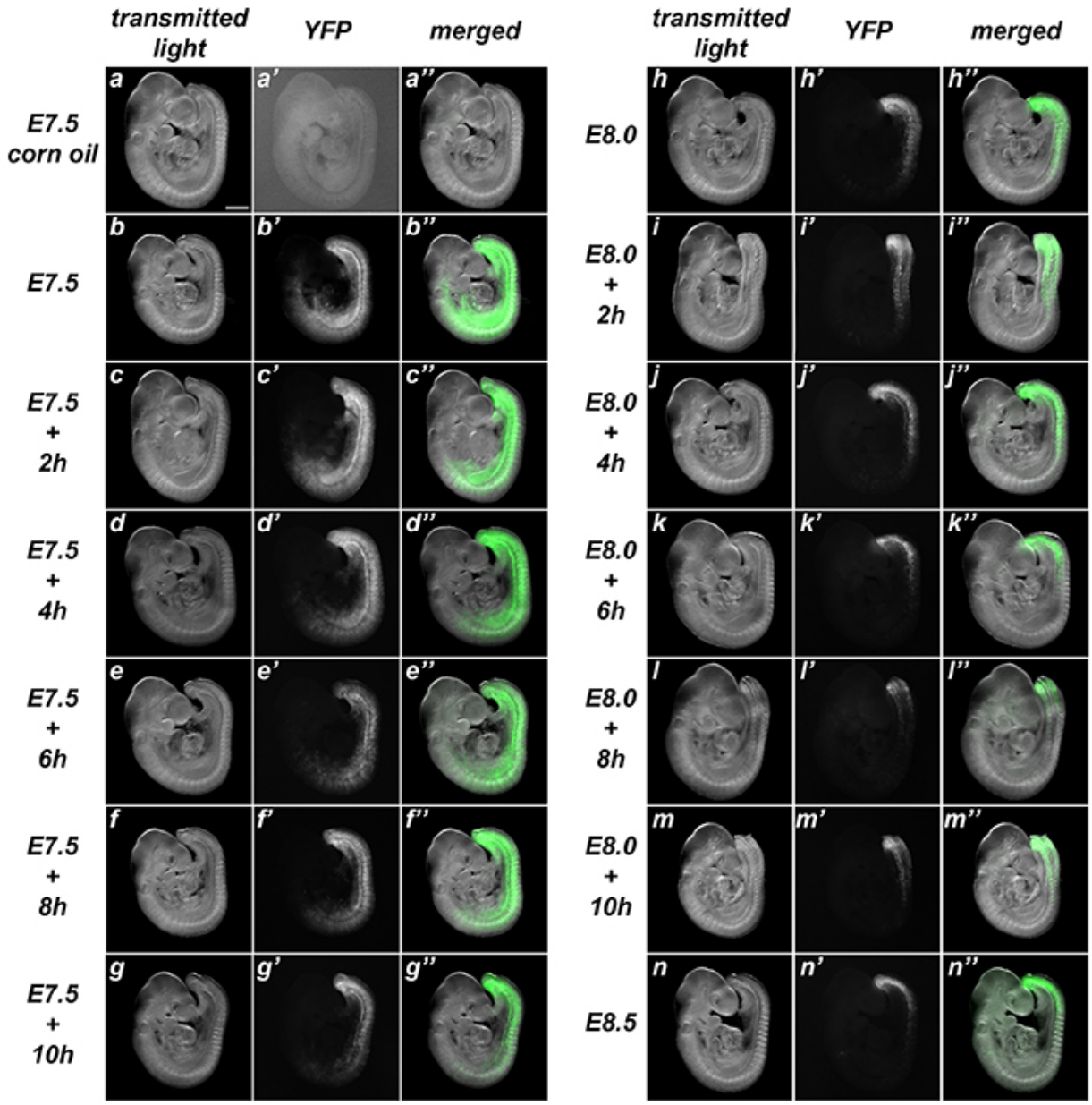

Supplementary figure 1. Characterization of the recombination activity of the *Tstr-cre^{ERT}* transgenics. These transgenics were analyzed by crossing them with ROSA26R-YFP mice. While non-treated embryos showed only rare events of spontaneous recombination (a), administration of tamoxifen at early stages induced extensive recombinant territories that got progressively restricted to the caudal region as tamoxifen was being administered at later time-points (b-n). Left rows adjacent to images show the time of tamoxifen administration. Size bar: 200 μm

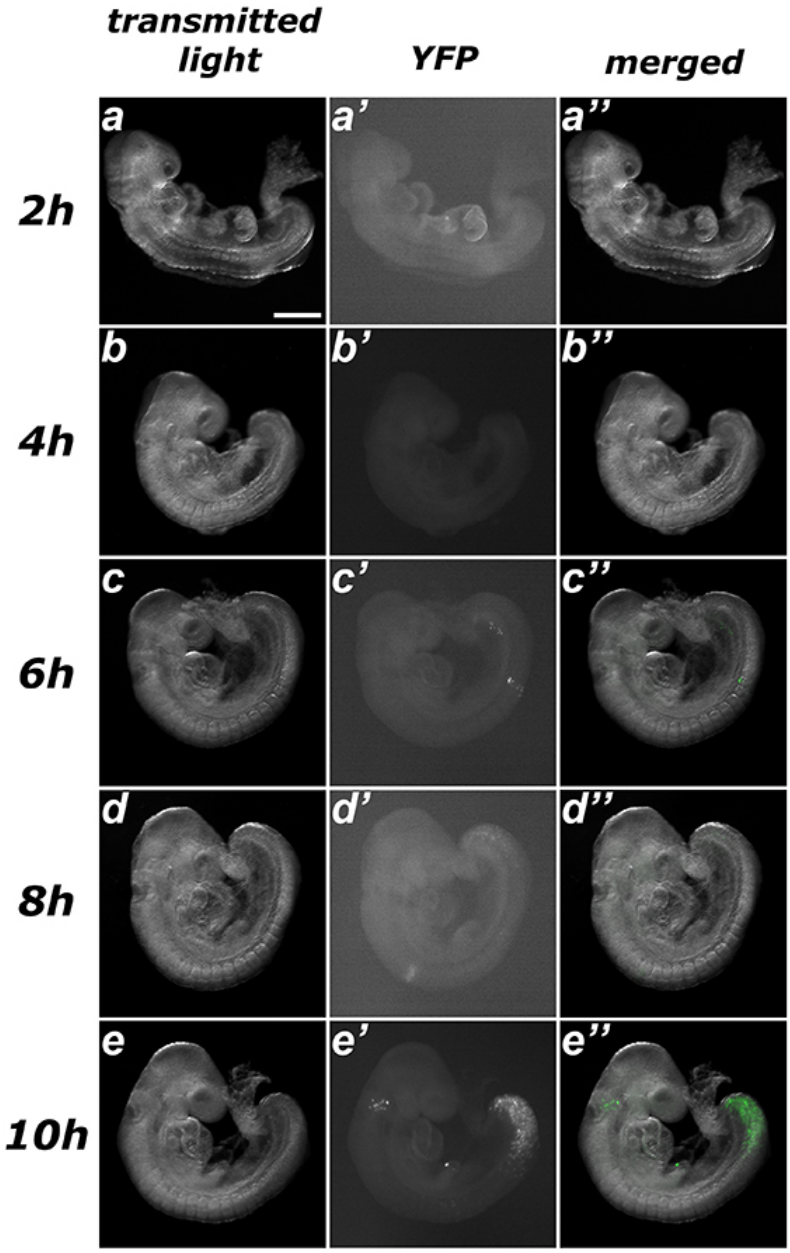

Supplementary figure 2. Estimating the time required for recombination after tamoxifen administration in Tstr-cre^{ERT}::ROSA26R-YFP embryos. No evident sign of recombination was observed after up to six hours of treatment (a-c), only a few scarce spontaneous events. Embryos harvested eight hours after tamoxifen administration exhibited early signs of recombination (d) and clear induction was observed ten hours after treatment (e). Size bar: 200 μm.

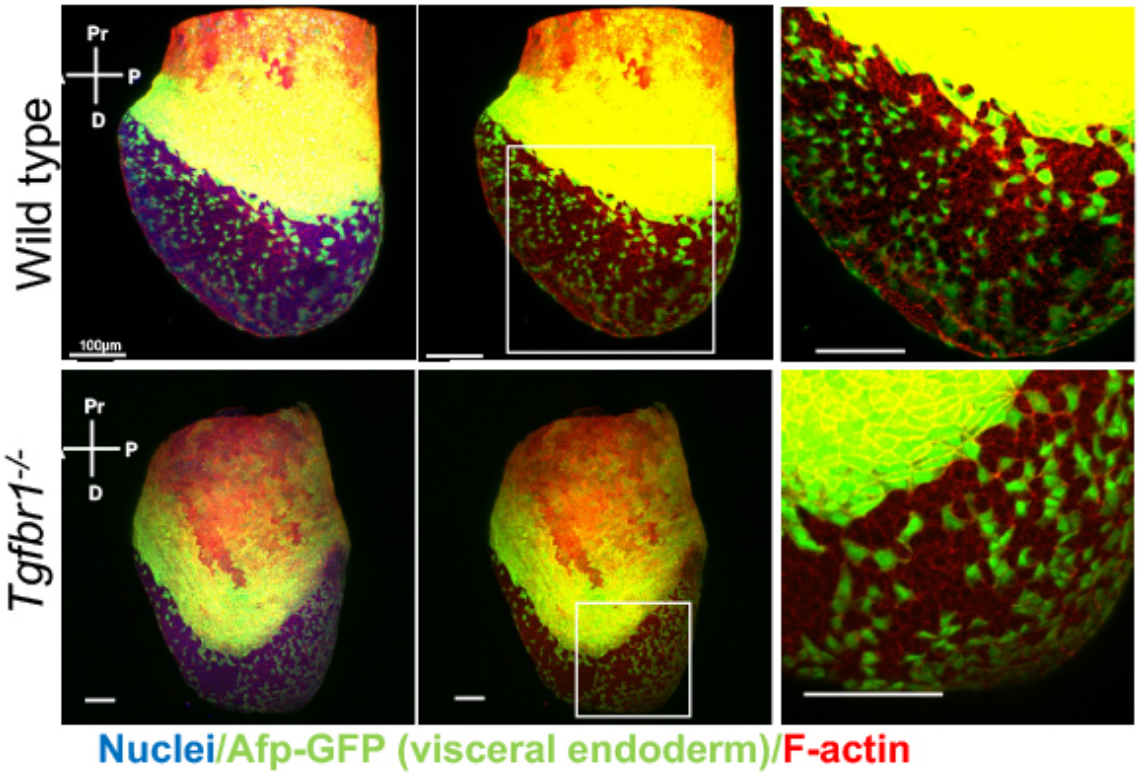

Supplementary Figure 3. Analysis of visceral endoderm (VE) dispersal in wild type and *Tgfbr1* mutant E7.5 embryos. No differences can be seen in the mutant embryo relative to the wild type control.

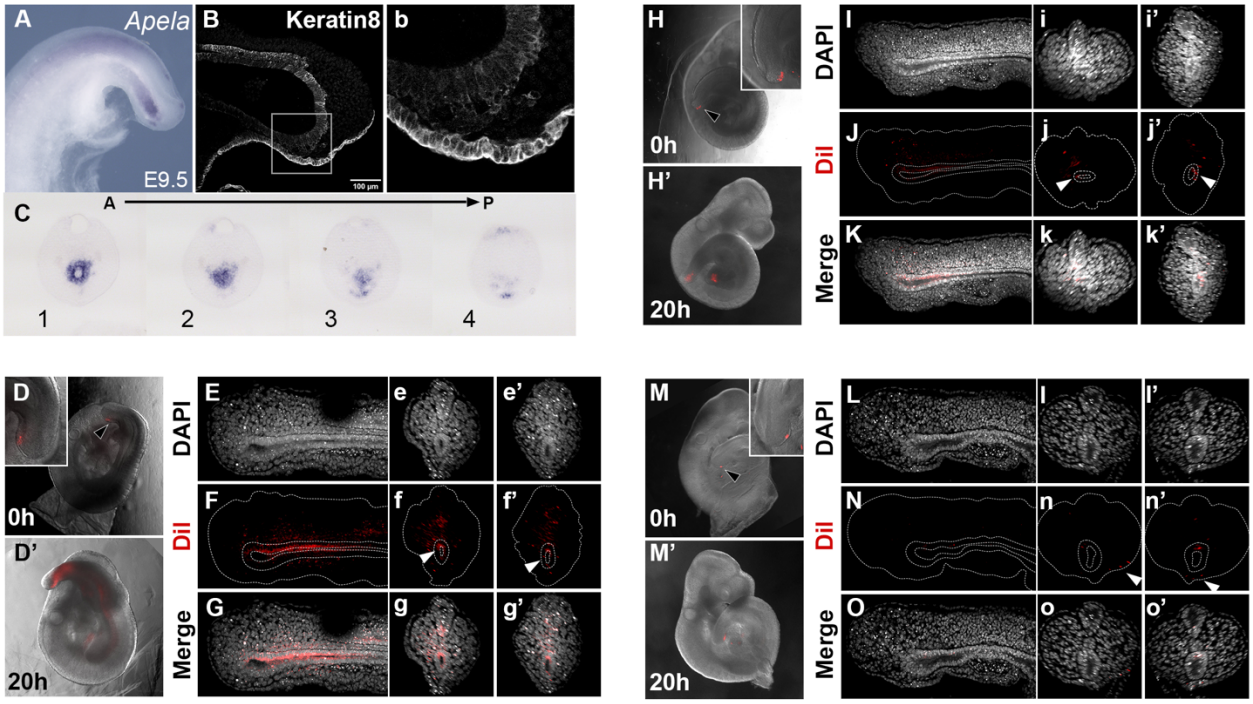

Supplementary figure 4. Dil labelling of the *Apela*$^{+}$ region in the E9.5 tail bud. A, C. *Apela* staining in the wild type tail bud at E9.5. C shows a series of transversal sections through the Apela-positive region shown in the whole mount image in A. **B, b.** Keratin 8 stained cells ventrally and posteriorly to the tail gut endoderm. b shows magnified image of the region marked by square in B. **D-o'.** Dil labelling of E9.5 embryos. Embryos shown in D-k' were injected in the region specified in b (black arrowhead). In M-o' Dil was injected in tailbud ectoderm (black arrowhead). D, D', H, H', M, M' shown whole mount images of embryos right after the injection (D, H, M) and after 20 h in culture (D', H', M'). Insets in D and H show that gut tube is negative for Dil staining. Inset in M show staining in the ectoderm. E-g', I-k' and L-o' show sagittal (E-G, I-K, L-O) and transversal (e-g', i-k', l-o') optical sections though the tail regions of cultured embryos shown in D', H', M' respectively. E-e', I-I', L-l' DAPI staining, F-f', J-j',N-n' Dil labelling, dashed line shows the outline if the tail and tail gut endoderm, G-g', K-k', O-o' – overlay of two channels. White arrowheads in f, f', j, j' shown incorporation of Dil-stained cells into gut endoderm whem mesenchyme was injected. When ectoderm was injected, Dil-stained cells contribute to ectoderm (white arrowheads in n, n'), and only minorly to gut endoderm and mesenchyme.

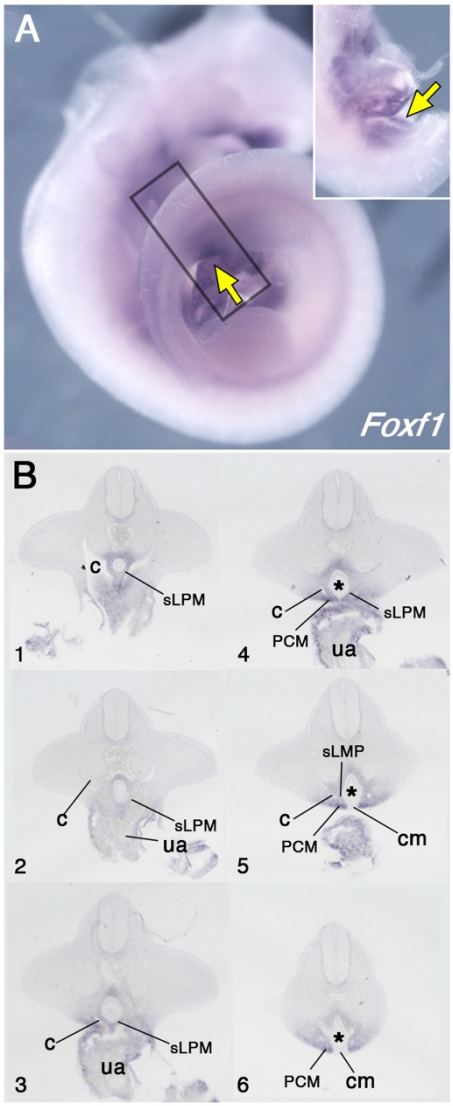

Supplementary figure 5. Pericloacal mesenchyme derives from the mesoderm adjacent to the allantois. A. Whole mount in situ hybridization hybridizations showing expression of *Foxf1* in E10.5 wild type embryo. Yellow arrows show expression in the pericloacal mesenchyme. Inset shows ventral view in the pericloacal mesenchyme. **B.** Series of transversal sections through the region marked by the rectangle in A (1-6, from anterior to posterior). Splanchnic LPM (sLPM) is separated from the pericloacal mesenchyme (PCM) by the coelomic cavity (c). Cloaca is labelled by asterisk, ua – umbilical artery, cm – cloaca membrane.